DEUTSCHES ELEKTRONEN-SYNCHROTRON DESY

DESY SR-79/26
October 1979

RADIATIVE AND NONRADIATIVE LIFETIMES IN EXCITED STATES OF Ar, Kr AND Xe ATOMS IN Ne MATRIX

by

U. Hahn and N. Schwentner
Institut für Experimentalphysik der Universität Kiel

NOTKESTRASSE 85 · 2 HAMBURG 52

To be sure that your preprints are promptly included in the
HIGH ENERGY PHYSICS INDEX ,
send them to the following address (if possible by air mail) :

DESY
Bibliothek
Notkestrasse 85
2 Hamburg 52
Germany

DESY SR-79/26
October 1979

Radiative and nonradiative lifetimes in excited states of Ar, Kr and Xe atoms in Ne matrix

U. Hahn[+] and N. Schwentner

Institut für Experimentalphysik der Universität Kiel,

Kiel, Germany.

Abstract

Synchrotron radiation with its intense continuum and its excellent time structure has been exploited for time resolved luminescence spectroscopy in the solid state. By selective excitation of n = 1, n' = 1 and n = 2 exciton states of Xe, Kr and Ar atoms in Ne matrix we were able to identify the emitting states involved. Lifetimes within the cascade of radiative and radiationless relaxation between excited states as well as the radiative lifetimes for transitions to the ground state have been derived from the decay curves. Energy positions and radiative lifetimes of the emitting states correspond quite well with those of the free atoms. Radiative and radiationless relaxation processes take place within the manifold of excited states of the guest atoms. The rate constants for radiationless decay confirm an energy gap law. The order of the radiationless processes reaches in some cases extremely high values. Selection rules for spin and angular momentum are essential to understand the observed radiationless transition rates.

[+] now at Deutsches Elektronen-Synchrotron DESY, Hamburg.

1. Introduction

The properties of rare gas solids have been studied extensively because they are prototypes for the large family of Van der Waals crystals [1]. The electronic states have been investigated by absorption, reflection and photoelectron spectroscopy [2]. In luminescence broad bands with a large stokes shift, sharp bands with a smaller red shift and in some cases resonant emission of free excitons have been observed [3]. The broad bands are attributed to the decay of selftrapped excitons which are similar to R_2^* excimers in the gas phase. The sharp bands correspond to quasi atomic excited states R^* which are induced by a bubble like relaxation of the surrounding atoms. Detailed experimental and theoretical results concerning the vibrational relaxation of the lowest free exciton states to the emitting states have been reported [3]. In rare gas solids pronounced exciton series up to members n = 5 are observed [2,3]. From the competition between relaxation in excitonic states and energy transfer to guest atoms a relative time scale for both processes has been derived [4].

Quantitative experimental results for electronic relaxation processes between excitonic states are missing. The reason is the extreme short time scale of these processes in pure rare gas solids which is caused by the fast depopulation of the excitonic states to the large number of branches of molecular potential curves formed in the selftrapping process to the excimer like centers [3]. By investigating the electronic relaxation in excited states of Xe, Kr and Ar atoms in Ne matrix, we have evaded this problem: For excited heavier rare gas atoms bound molecular states with Ne atoms do not exist and therefore in the Ne matrix relaxation to a manifold of excimer states is excluded. On the other hand

the lowest excited states in Ne form for each species of guest atoms an exciton series which is very similar to the matrix exciton series. This allows the study of electronic relaxation within exciton states by exciting the guest atom only.

Electronic relaxation has been investigated for excited states of rare earth ions doped into insulator crystals for transitions in the visible and infrared [5]. The energetic position of the excited rare earth states depends on the crystal field determined by the matrix. Transitions with low oscillator strength corresponding to radiative lifetimes from μsec to msec determine the time scale. We show that for the heavy rare gas atoms in Ne matrix - after vibronic relaxation of the matrix - the well-known atomic states of the guest atoms are involved. The times for the observed transitions lie in the nsec regime and the concepts for radiationless transitions may be tested in an extended region.

Matrix isolation spectroscopy of excited molecular states in rare gas matrices gains new interest due to the development of selective excitation sources in the vacuum ultraviolet like vacuum ultraviolet lasers and synchrotron radiation. The interpretation of relaxation processes in the complex molecular states can be guided by the experiences on the much simpler atomic systems.

Exciton states of guest atoms in Ne matrix are well suited for the study of electronic relaxation processes:

i) Due to the large exciton binding energies the emission bands of the different members in the series are well separated in energy.

ii) The series of guest atoms Ar, Kr, Xe allows a systematic change of energy spacings in the involved guest atom states.

iii) The monotonic increase in the strength of spin orbit coupling from Ar to Xe allows a systematic study of the matrix element for spin conversion in radiationless relaxation processes.

2. Experimental Techniques

The experiments were performed with the radiation of the storage ring DORIS at the Deutsches Elektronen-Synchrotron DESY in Hamburg. In the following we emphasize only those aspects of the set-up of particular importance for the experiment. The experimental arrangement has been described in detail elsewhere [6,7].

(A) Experimental setup

The synchrotron radiation is monochromatized by a 1 m modified Wadsworth monochromator providing 10^8 to 10^{10} photons/Å sec in a wavelength region from 400 Å to 2000 Å at the site of the sample with a resolution of about 1 Å. The light from the monochromator is focussed by a toroidal mirror onto the sample. The image serves as the entrance slit for a 0.3 m windowless Seya-Namioka secondary monochromator providing a resolution of 15 Å (Fig. 1). For the measurements reported here a dual channel plate from Varian which gives excellent time resolution has been used [7]. Count rates of 10^3 counts/sec in the emission bands were typical. The sensitivity of the channel plate ($\sim$ 10 % at 1000 Å) decreases to longer wavelengths. For the calculation of branching ratios and corresponding relaxation times the

intensity in the emission bands has been corrected for the wavelength dependence of the sensitivity.

(B) Determination of time constants

The high energetic electrons in the storage ring DORIS form bunches with a length of 3.96 cm. The geometrical length of the electron bunches causes synchrotron light flashes of 130 psec fwhm with a Gaussian shape. The ring can be filled with 1 bunch or up to 480 bunches. During the period of the experiments the separation between the light flashes has been 8 nsec in the 120 bunches mode and 1 μsec in the single bunch mode. At a count rate of $\simeq 10^3$ counts/sec and a repetition rate of excitation pulses of 1 MHz up to 125 MHz only after 10^3 up to 10^5 excitation pulses one luminescence light pulse is detected. For these conditions the single photon counting and timing technique [8] is the most appropriate method to determine luminescence lifetimes. A pulse from the channel plate starts a time to amplitude converter and a reference pulse obtained from the high frequency oscillator of the storage ring provides the stop signal. The voltages from the time to amplitude converter are stored in a multichannel analyser and the resulting decay curves are then handled in a computer. The general evaluation of the experimental curves is described in the appendix. The further simplifications for each individual cascade which follows from the experimental results are discussed with the presentation of the data.

(C) Sample preparation

The samples have been prepared as thin films by deposition onto a copper substrate which has been cooled by a liquid Helium flow cryostat.

The background pressure was 10^{-9} torr and lower. The gases for the doped samples have been mixed in a ultra high vacuum gas handling system with partial pressures according to the indicated concentrations. Gases with a purity of 99.997 % for Ne, 99.9997 % for Ar, 99.997 % for Kr and 99.997 % for Xe delivered by Messer Griesheim have been used without further purification. The deposition temperature was 5 ± 1 K. Annealing up to 9 K did not influence the emission spectra. The concentration of the guest atoms has been chosen small enough for the spectra presented here to ensure that only emission from monomer guest centers takes place. We checked that no emission in the well-known dimer emission bands appears.

The film thickness of our samples has been increased until the emission intensity saturated when the samples have been excited in the dominant absorption structures of the guest atoms. The estimated thicknesses lie between 1μ and 100 μ. Under these conditions no contributions of additional impurities in the bulk have been detected. This has been confirmed by a comparison with samples doped with atmospheric gases (N_2, O_2, CO, H_2). Emission spectra and decay times showed no change for hours after the deposition. Also the absolute intensities and the decay times are reproducible for independently prepared samples. This shows that surface quenching which is critical for pure rare gas solids [3] is negligible when guest atoms are excited directly. The mean distance of excited guest atoms to the surface is large when excitation light with energies in the transparent region of the Ne host is used. This is due to the small guest atom concentration.

3. Experimental Results

First the samples have been excited with the white light from the primary monochromator in zeroth order to populate all possible emitting states. These emission spectra give a survey of the emitting states. Then appropriate excitation energies have been chosen to get a complete set of emission spectra for all three kinds of guest atoms (Fig. 2). The shape of the bands is broadened by the experimental resolution of 15 Å which is indicated in the eV scale for Kr/Ne in Fig. 2. For each kind of guest atoms three emission bands I, II, III are observed. The width of the lower one's I and II is determined by the resolution. For Ar in Ne the bands I and II have not been separated completely. For excitation energies of 12.5 eV and 12.73 eV only either the lower or higher one of the two emitting states is populated, allowing the separation of band I and II as shown by the dashed lines in Fig. 2. The emission bands III are definitely broader than the experimental bandwidth. The relative intensities in Fig. 2 are multiplied by the attached factors.

In the next step the intensity in each emission band has been measured as a function of excitation energies. These excitation spectra show which primarily excited electronic states contribute either directly or via relaxation processes to the chosen emission band. Fig. 3 shows the results for Xe/Ne. From the emission spectrum (see inset and Fig. 2) the lowest emission band I has been chosen and the intensity versus excitation energy is presented as the hatched curve in the lowest row of Fig. 3. For

comparison the emission band is shown on the same energy scale. Evidently there is only one electronic state contributing to the emission band and no relaxation from higher excited states to the emitting state takes place. The separation of the excitation maximum and of the emission maximum immediately gives the stokes shift between excited state and emitting state. In the next two rows the excitation spectra of the emission bands II and III are given in the same way. For these emissions a stokes shift but also relaxation from higher excited states is observed.

We expect a close similarity between excitation and absorption spectra because the finite film thickness yields complete absorption of the penetrating light only for high absorption coefficients. Therefore the excitation spectra allow to identify the excited states of guest atoms in the Ne matrix similar to absorption spectra. Furthermore the relative intensities at one special excitation energy in the excitation spectra of the three emission bands give the branching ratio for relaxation from the primarily excited state to the three emitting states. For example for the excitation energy of 11.54 eV (maximum d) no relaxation at all to the emitting state I and a branching of 2 : 1 to bands II and III is observed. The relative scale for the intensities in II and III has to be taken from the emission spectrum in the insert.

Finally for each emission band the time dependence has been measured at prominent excitation energies. The logarithm of the intensity versus the time in nanoseconds for the excitation energies indicated by a, b, c, d, e is presented for each emission band at the end of each row in the inserts

of Fig. 3. The decay curves are plotted on a larger scale in Fig. 6. The dark current was ∿ 10 counts/channel. The results for Kr and Ar are shown in a similar way in Fig. 4,5,7 and 8.

The maxima in the excitation spectra i.e. the energy positions of the primarily excited states are collected in table 1 and compared with absorption results. The energies of the emission bands are listed in table 2. The relative intensities of the emission bands I, II and III for the excitation channels a, b and c are collected in table 3.

The rise and decay times in the decay curves are the times for population and depopulation of the excited state. They have been determined from fits of the experimental curves with a combination of exponential terms as described in the appendix. With one exception all curves have been fitted with only one rise time, one decay time and if necessary with a constant background. The exception is curve Ic in Fig. 8 for Ar. Here a small contribution with the life-time of 12 nsec of the emission band II had to be included in the rising part of the curve. The reason is the small separation of emission I and II which has not been resolved completely as has been mentioned above. If two time constants are sufficient to fit the data then it is obvious to try a three level system where only the two life-times τ_1 and τ_2 remain as parameters (see appendix). This fitting procedure has been successful except for the curve Ib in Fig. 7. for Kr. In this case resonant energy transfer distorts the simple decay as will be discussed later. The curve Ib of Kr required a positive ratio of 0.1 for the preexponential factor instead of - 1 (see appendix). The constant background in some of the curves belongs to the sublevels as described in the appendix. The final

fits are shown in Fig. 6,7,8 together with the experimental points. The time constants and the relative intensities of the background to the short components are collected in table 3.

As we have more experimental data than necessary we have been able to check the consistency of the model and of the evaluated time constants (see appendix). We considered also more complicated models with intermediate levels between the $n = 2$ and $n' = 1$ excitons. But reasonable fits have been only obtained with the models which are presented here. The reason that only two time constants contribute to each decay curve is due to the fact that from all possible decay channels only very few are active. The explanation will be given in the later discussion of each individual cascade.

In this paper we are concerned with the luminescence properties of rare gas atoms in Ne matrix and the relaxation processes in the excited states of these atoms. Therefore only results for photon energies below the first absorption band of the Ne matrix at $\hbar\omega = 17.6$ eV are presented. At higher photon energies predominantly the matrix will be excited. Then a competition between relaxation in the Ne matrix, emission of Ne and energy transfer to the guest atoms with relaxation in the guest atoms will be observed. These complex processes may be analysed later when the processes solely in the guest atom states are understood.

4. Atomic impurity states in excitation and emission

(A) Excitation spectra - Wannier states

The absorption spectra of Xe, Kr and Ar atoms in Ne matrix have been investigated up to 12 eV by Baldini [9] and to higher energies by Pudewill et al. [10] and interpreted as atomic impurity Wannier states showing two series of excitations up to members n = 5. The two series are separated by the spin orbit splitting of 1.3 eV, 0.64 eV and 0.2 eV for excitation of Xe, Kr and Ar atoms, respectively. For members $n \geq 2$ the energies can be fitted by a hydrogen like Wannier series. The binding energies of the excitons E_n^i turn out to be the same as the binding energies E_n of the matrix excitons (equ. 1). Thus the binding energies for $n \geq 2$ are independent of the special guest atoms which only determines the spin orbit splitting and the convergence limit E_G^i of the series.

$$1) \quad E_n^i = E_n = \frac{B}{n^2} \quad \text{for } n \geq 2 \text{ where i stands for Ar, Kr and Xe atoms}$$

This observation is the basis for using the effective mass approximation for binding energies of atomic impurity states:

$$2) \quad B = \frac{e^4}{2\hbar^2\varepsilon^3}\mu$$

In this approximation the binding energies depend only on the dielectric constant ε which for the large radius of $n \geq 2$ excitons will be the matrix ε and the reduced effective mass μ of electron and hole states. Due to the large mass of the hole states of the flat Ne valence band and of the localized impurity states, μ can be approximated by the electron mass for guest and matrix states. This mass is determined mainly by the extended matrix

conduction band states.

The small radius of the n = 1 excitons requires in the effective mass approximation a so called central cell correction for a local dielectric constant and reduced effective mass, or it can be accounted for by using a tight binding approximation [11]. The energy levels measured by absorption are collected in Fig. 9 and in the right rows of table 1 where the excitation energies $\hbar\omega_n^i$ are given by

$$3) \quad \hbar\omega_n^i = E_G^i - E_n^i$$

The whole set of maxima for the emission bands I, II and III in the excitation spectra of Figs. 3,4,5 represents an independent measurement of the energetic position of excited guest atom states (table 1). The experimental data are compared with calculated ones, using the recently reinvestigated Ne exciton binding energies [11]. The energies $\hbar\omega_2^i$, $\hbar\omega_2$ of the n = 2 excitons serve as reference.

$$4) \quad \hbar\omega_n^i = \hbar\omega_2^i + \hbar\omega_n - \hbar\omega_2$$

For those exciton states where values by Baldini and Pudewill et al. are available there is agreement within 0.1 eV. Additionally we have been able to identify higher members of the exciton series especially for Xe/Ne up to n = 5. The agreement with the excitation energies calculated from the Ne exciton binding energies is good within the reproducibility of our results. It confirms the concept of the effective mass approximation for these atomic impurity states.

In the excitation spectra a fine structure in the region of the n = 2 and n' = 2 exciton states appears which has not been reported previously. The origin of this fine structure is not clear. Some structures in the spectra of Pudewill et al. have not been identified too. The structures between n' = 1 exciton and n = 2 exciton observed for Xe in Ne will be assigned later to 5d transitions.

(B) Emission spectra - atomic states

For each kind of guest atoms the energies of the three emission bands I, II and III are listed in table 2. The bands I and II (except II in Kr) have been also observed by Gedanken et al. [12], Fugol [13] and Schuberth et al. [14]. The bands III are reported for the first time (table 2). Within a blue shift of 0.1 to 0.2 eV the emission bands I in the Ne matrix agree with allowed radiative transitions from the 4s state in Ar, the 5s state in Kr and 6s state in Xe. In the same way the emission bands II are attributed to the dipole allowed transition of the ns' atomic states to the ground state. Therefore a matrix relaxation around the excited atoms has been postulated which leads to emission centers similar to excited free atoms. Also the new bands III can be correlated within a blue shift of 0.2 eV with dipole allowed transitions either from the 3d state for Ar, 4d state for Kr and 7s or 5d state for Xe (see Fig. 2).

Until now the assignment to atomic states is based only on the approximate coincidence of the energies. Our results for the lifetime of these states give clear evidence for the relation to the atomic states due to the similarity in the oscillator strengths. To get the transition rates to the ground states the influence of cascading processes has to be considered.

The contribution of states to the bands III depends strongly on the competition of relaxation processes, therefore these bands will be discussed later. The population of the fine structure components observed by Schuberth et al. (table 2) in bands I and II is due to relaxation from higher excited states and will also be discussed later. In earlier luminescence investigations only unspecific excitation by α particles or x-rays has been used, thus cascading in the large spectrum of excited states cannot be avoided. From the excitation spectra we know the lowest excitation energy of each emission band. Thus we are able to populate the emitting electronic states selectively.

The decay times for the emission bands I ($1s_4$) are listed in table 4. These bands correspond to the lowest allowed transitions. A background due to long decay times of the metastable ($1s_5$) states is not observed and non-radiative relaxation to the ground state on a time scale of nanoseconds is not expected for energy differences of 8 eV and more. Therefore it is justified to take the decay times as the radiative decay times to the ground state. For excitation of the n' = 1 states of Xe and Ar only band II is observed. With the arguments given above there is no decay process competing with the radiative decay to the ground state. The decay times of these bands ($1s_2$) given in table 4 are again the radiative lifetimes. In Kr for excitation of n' = 1 states a branching in emission I and II is observed and from the relative intensities together with the decay time of 1.2 nsec, the radiative decay time to the ground state is derived and given in table 4. These radiative lifetimes for Xe and Kr in the Ne matrix agree quite well with recent lifetime measurements in the gas phase (table 4). For a quantitative comparison with the gas phase values a correction for the local field has

to be introduced. In the literature different local field corrections are discussed [15,16]. Further the correct combination and choice of the refractive indices of the host and guest is ambigious. Using the expression given by Person [15] and refractive indices n_o = 1.23 of the Ne matrix and n = 1.30 for Ar n = 1.39 for Kr and n = 1.54 for Xe we get the corrected values of the table 4. The values in brackets correspond to values n_o = n = 1.23 of the matrix. The correction is not essential, but applying it gas phase and matrix values agree within 0,5 nsec for Xe and Kr. The larger difference for Ar can be partly due to the gas phase values which have been determined from the oscillator strengths in absorption experiments. Similarily earlier Xe and Kr gas phase values scattered by some nsec. The ratio of the lifetimes of band I to band II corresponds quite well to the ratio of the Ar 4s to 4s' lifetimes.

The lifetimes of the allowed ns states $1s_2$ and $1s_4$ could be shortened by relaxation to the metastable $1s_3$ and $1s_5$ states. Due to the long lifetimes of the metastable states, a population of these states by relaxation would cause a long background. Such a background is observed for Ar and Kr when n = 2 excitons are excited but not for direct population by n = 1 and n' = 1 excitation (see later). Therefore such a shortening of the observed lifetime (table 4) relative to the true radiative lifetime is at least less than 10 %. This is different to the case of Kr atoms in Ar matrix. In the Ar matrix a relaxation from $1s_4$ to the metastable state $1s_5$ has been observed, but not from $1s_2$ to $1s_3$ [17].

Finally we want to summarize

i) in excitation spectra we observe impurity states mainly determined by the matrix and well described by a solid state picture i.e. the effective mass approximation with a central cell correction for the n = 1 exciton states;

ii) in emission spectra the states are quite well described by the blue shifted free atomic states of the guest atoms.

5. Radiative and non-radiative relaxation cascades in excited atomic impurity states

(A) Experimental relaxation cascade

The discussion of relaxation processes will be restricted to the cascade of n = 1, n' = 1 and n = 2 excitons. The decay times for excitation to higher excited states do not allow to give quantative values for the relaxation of the higher excited states to the n = 2 state and to the lower states because the relaxation is too fast compared with the accuracy of our decay time measurements. Differences of less than 0.1 nsec for typical decay times of some nsec cannot be distinguished from experimental errors. On the other hand the time resolution for decay time themselves is of the order of 0.01 nsec.

First we have to connect each emitting state to the electronic state where it is originating from. The lowest excitation energy for an emission band immediately shows the corresponding electronic state. According to table 1

and Figs. 3,4,5 the n = 1 excitons are converted to the 4s, 5s and 6s atomic states, the spin orbit partners n' = 1 to the 4s', 5s' and and 6s' atomic and the n = 2 excitons to (n + 1) s or nd states of Ar, Kr and Xe, respectively. The appropriate description for the matrix relaxation of these localized centers is a configuration model where in first approximation the mean separation of the guest atom to the nearest neighbours of matrix atoms can be used as a configuration coordinate. The energies and the oscillator strengths of the emitting states are close to the atomic values therefore a relaxation of the neighbouring matrix atoms to a larger separation from the excited guest atoms has been postulated qualitatively. Thus a bubble with a larger configuration coordinate is formed around the excited atom. This kind of centers has also been discussed as one possibility of relaxation around excited atoms for pure rare gas solids [13]. Quantitative values for the separations in this configuration model should be based on investigations of the local structure around the guest atoms in the ground and in the excited states which are missing until now. Absorption to the n = 1, n' = 1 and n = 2 exciton states will take place at the equilibrium configuration coordinate of the ground state. Then the energy is lowered by the matrix relaxation. The stokes shifts between absorption and emission of 0.2 to 0.8 eV (table 2) are due to the depth of the potential curves in the excited states and the contribution due to the repulsive ground state at the equilibrium position of the excited states (see for example Fig. 10). Adopting the values for Ne [13] the second part should be small and most of the stokes shift is caused by the relaxation energy of the excited state.

In table 3 all experimental rise times and decay times are presented. When the emitting state is populated directly by absorption into its corresponding electronic state (n = 1 for band I; n' = 1 for band II and n = 2 for band III) then the rise time is extremely short for all guest atoms. It is too short to be the decay time therefore it gives the time for populating the emitting state by the matrix relaxation. The time is shorter than our experimental resolution and only an upper limit of 0.01 nsec can be derived. This relaxation is based on electron-phonon interactions and can be handled by multiphonon theory [3a]. The large red shift between absorption and emission bands, the large line widths of the absorption bands [3] and a line shape analysis by Ophir et al. [18] indicate strong electron-phonon coupling. Such lattice relaxation processes are expected to occur on a time scale of 10^{-13} sec in accordance with our experimental result.

As can be seen from table 3 the time for matrix relaxation is much shorter than all decay processes. Therefore it is justified to assume as a first step a complete matrix relaxation and to discuss the competition between radiative and radiationless decay processes from the relaxed quasi atomic states. Thus the cascade can be reduced as is illustrated in the appendix and as is worked out for Xe, Kr and Ar in Figs. 10, 11, 12. On the left hand side of Figs.10, 11 and 12 the experimental values for the cascade are illustrated (table 4 and 5). They are derived from the combined information contained in the excitation spectra, the emission spectra and the rise and decay times (table 3). Population of the n = 1 exciton is followed simply by radiative decay. For the n' = 1 excitons of Xe and Ar also only radiative decay is observed. From the statistics in the excitation spectrum of band I a lower limit for the relaxation time constant between n' = 1 and n = 1 of 100 nsec is derived in both cases.

In Kr a branching into band I and II is observed after n = 1 excitation. With the lifetime of 1.2 nsec taken from curve IIb in Fig. 7 and with the intensity ratio of band I and II (table 3) a time for relaxation from $1s_2$ to $1s_4$ of 1.9 nsec and a radiative lifetime of 3.1 nsec is calculated. But we have the problem that curve Ib of Fig. 7 cannot be fitted with the simple cascade formula as has been mentioned in part 3. We observe in Ib a much faster increase than is obtained with the lifetime of 1.2 nsec of the $1s_2$ state in the 3 level system. For Kr the emission band II nearly coincides in energy with the absorption band of the n = 1 exciton. Therefore a distortion of the results due to reabsorption of the band II simulating relaxation from II to I would be possible. We do not believe that reabsorption is the major contribution.

First, we excite in the n' = 1 absorption band and its absorption coefficient is comparable to that of the n = 1 band. Therefore the distribution of the light in the ensemble of guest atoms does not favour reabsorption to a larger extent. This may be different for experiments with x-ray and α-particle excitation.

Secondly if we would assume strong reabsorption and little relaxation to explain the branching into band I and II after n' = 1 excitation of Kr atoms than we would have to take the measured time of 1.2 nsec as the radiative lifetime of the $1s_2$ state in the matrix. This time would be much faster than the corresponding atomic, radiative lifetime which does not fit to the whole picture derived for the radiative lifetimes.

Thirdly, with reabsorption we also cannot explain the short rise time curve Ib.

Besides relaxation and reabsorption resonant energy transfer has to be considered. Due to the matrix relaxation the $1s_2$ state becomes energetically resonant with the n = 1 absorption band of Kr atoms surrounding the excited Kr atom. For these strongly localized centers the Förster Dexter Dipol-Dipol energy transfer mechanism is appropriate. By convoluting the time dependence of the donor emission $n_D(t)$ (equ. 5) with the experimental response function we are able to fit the time dependence of the emission band II (IIb in Fig. 7) using the atomic radiative lifetime $\tau_{10} = 3.1$ nsec of the $1s_2$ state and a value of $2b = 5 \times 10^4\ \mathrm{sec}^{-1/2}$.

$$5) \quad n_D(t) = n_D(0) \exp\left(-t/\tau_{10} - 2b\sqrt{t}\right)$$

With this value of 2 b and the previously determined radiative lifetime $\tau_{20} = 2.5$ nsec of the $1s_4$ state which is the relaxed n = 1 acceptor state, all parameters in the time dependence of the acceptor emission $n_A(t)$ are known (equ. 6).

$$6) \quad n_A(t) = n_D(0) \frac{2b}{\sqrt{\gamma}}\, \omega\left(\frac{b}{\sqrt{\gamma}}\right) \exp(-t/\tau_{20}) + \omega\left(\sqrt{\gamma t} - \frac{b}{\sqrt{\gamma}}\right) \exp\left(-t/\tau_{10} - 2b\sqrt{t}\right)$$

$$\gamma = 1/\tau_{10} + 1/\tau_{20}$$

$$\omega(z) = e^{-z^2} \int_0^z e^{x^2}\, dx$$

Indeed curve Ib in Fig. 7 is nicely described by this expression when the experimental response function is included. This energy transfer process provides a steep enough rising of the emission in curve Ib and it fits the two independent measurements IIb and Ib with the same parameter 2b. With the concentration $N_A = 4 \times 10^{+19}$ cm^{-3} (0.1 %) which has been used in the experiment, a Förster Dexter radius of $r_o = 21$ Å is obtained from the experimental 2b value (equ. 7).

7) $2b = \frac{4\pi}{3} \sqrt{\pi C} \cdot N_A$

$C = r_o^6 / \tau_{10}$

The value is quite reasonable for this allowed dipole transition. Finally from r_o and N_A an intensity ratio of 3 is calculated for the emission bands I and II which has to be compared with the experimental value of 1.6 (table 3). We believe that this deviation by a factor of 2 is not serious particularly because we have used one single concentration. We conclude that the dominant process responsible for the branching into bands I and II after n' = 1 excitation in Kr is resonant energy transfer. Direct relaxation between $1s_2$ and $1s_4$ within the same excited Kr atom does either not take place or gives only a small contribution to this branching. We cannot completely exclude it and state that the relaxation time constant for $1s_2 \rightarrow 1s_4$ is longer than 1.9 nsec.

A very essential observation is that for all three species of guest atoms Xe, Kr and Ar no relaxation at all has been observed between the manifold of $1s_2$, $1s_3$, $1s_4$ and $1s_5$ states (table 5) except the not completely clear case of the $1s_2 - 1s_4$ transition for Kr. This experimental fact gives strong

arguments that selection rules are very important for radiationless transitions.

Next excitation of n = 2 excitons has to be discussed. For Xe population of n = 2 simply gives a branching into bands II and III and no relaxation to n = 1 is observed. Again a lower limit for the relaxation time n = 2 to n = 1 of 100 nsec is obtained. The lifetime $\tau_1 = 0.57$ nsec of the relaxed n = 2 states (see appendix) is caused by the depopulation due to the radiative decay τ_{10} and the relaxation τ_{12}.

8) $1/\tau_1 = 1/\tau_{10} + 1/\tau_{12}$

Using in addition the intensity of the bands II and III we can calculate the radiative decay time τ_{10} of 1.3 nsec and the relaxation time τ_{12} of 1.0 nsec. The experimental data are consistent: the lifetime of the n = 2 state appears as population time for the n' = 1 state and n' = 1 again decays with its radiative lifetime within the experimental accuracy (table 3). Finally as mentioned before no significant changes are observed when higher excited states (Fig. 3,d and e) are populated.

For Kr and Ar population of n = 2 excitons leads to a more complicated cascade. Additional to the radiative decay and to the relaxation n = 2 $\rightarrow$ n' = 1 a relaxation to n = 1 is observed.

Now the lifetime τ_1 of the upper level appears as the decay time of n = 1 and the radiative lifetime of n = 1 as its rise time. The time dependence of the luminescence is symmetric in population and depopulation. The criterion

is the relative magnitude of the time constants and now the population times of 6 nsec for Kr and 13 nsec for Ar are longer than the corresponding radiative lifetimes of 2.5 nsec and 4.7 to 5.8 nsec. The same inversion is observed for the n' = 1 state of Ar after n = 2 population. For Kr this decay curve has not been measured because of the low intensity of band II (Fig. 4).

For Ar τ_{23} is zero. We can calculate (see appendix) the radiative lifetime τ_{10} and the relaxations times τ_{13} and τ_{12} from the lifetime τ_1 and the relative intensities of the bands III, II and I (table 3).

9) $1/\tau_1 = 1/\tau_{10} + 1/\tau_{13} + 1/\tau_{12}$

10) $F_3/F_1 = \tau_{10}/\tau_{13}$

$F_2/F_1 = \tau_{10}/\tau_{12}$

For Kr we have to use the expressions for the 4 level system from the appendix to include the transfer $1s_2 - 1s_4$. In the case of n = 2 excitation of Kr an additional background appears in the decay curves of emission band I (Fig. 7, Ic; and table 3). This fact shows that two states $1s_4$ and $1s_5$ are populated which are closer together in energy than the experimental energy resolution. These two states are distinguished by their radiative decay times to the ground state. For the allowed transitions from $1s_4$ to the ground state the radiative lifetime is 2.5 nsec.

The forbidden transition from the metastable $1s_5$ state is responsible for the constant background. When the $1s_4$ state is populated directly by light via n = 1 excitation no background is observed because no relaxation $1s_4 - 1s_5$ takes place. Therefore the branching ratio for the relaxation τ_{1s_4} and τ_{1s_5} is simply given by the intensity ratio of the 2.5 nsec component to the background (table 3) using the previous determined τ_{13} (see appendix).

For the case of n = 2 excitation of Ar such a background has been observed in both emissions I and II (Fig. 8: Ic, IIc). In the same way the branching ratio for the relaxation times τ_{1s_2}, τ_{1s_3}, τ_{1s_4}, τ_{1s_5} are calculated. The evaluation is so simple because no relaxation between the fine structure components has to be considered. The relaxation time constants are summarized in table 5.

(B) Discussion of the relaxation cascade

In the discussion of the relaxation cascade three main ingredients will be used:

i) Relaxation takes place within the set of atomic states of the guest atoms.

ii) Radiative decay between the excited atomic states and to the ground state takes place similar to that observed for free atoms

iii) Nonradiative decay obeying the usual energy gap law competes with radiative decay processes.

As has been shown before and as follows from the fine structure observed by Schuberth and Creuzburg [14] (see 6.) the approximation

of the emitting states by the atomic states is reasonable, despite the blue shifts and the shifts in the fine structure. Even the matrix elements for radiative decay are similar enough within the expected accuracy. Therefore it seems justified to use also all the other components of excited atomic states as illustrated in the right parts of Figs. 10, 11, 12. The atomic fine structure is well investigated in the gas phase [19] and most of the radiative rate constants for the stronger transitions between these states are known [20]. In the figures the states with dipole allowed transitions to the ground state are marked by large bars together with the radiative decay time. Further the lifetimes for the strongest transitions to the lower excited states are indicated. Within our discussion we neglect field corrections and assume the same rate constants in the matrix. We will show the importance of nonradiative decay which is in competition to the radiative decay channels. Rate constants for nonradiative decay are generally derived from the so called "non adiabatic hamilton method" (see for example the survey of Auzel [21]. It allows to separate a rate constant W into a term C^2 containing predominantly electronic matrix elements which follow from the symmetry of the two electronic states involved and a second term containing Frank Condon factors which describe the dissipation of the electronic energy difference ΔE into the phonon system of the matrix. With crude but from the comparison with experiments well established approximations the second term can be written in the following way for the two limiting cases of strong (equ. 11) and weak coupling (equ. 12). We use the notation of Englman and Jortner [22]. For E_A and E_M see Fig. 13.

$$11) \quad W = \frac{C^2\sqrt{4\pi}}{\sqrt{E_M \hbar\langle\omega\rangle}} \exp\left(-2E_A/\hbar\langle\omega\rangle\right)$$

$$12) \quad W = \frac{C^2\sqrt{2\pi}}{\hbar\sqrt{\hbar\omega_M \Delta E}} \exp\left(-\gamma\Delta E/\hbar\omega_M\right)$$

Here the low temperature limit according to our experiment is used and $\langle\omega\rangle$ corresponds to a mean phonon energy and ω_M to the maximum phonon energy of the system guest atoms and matrix. The parameter γ(equ. 5.6 in Englman and Jortner) contains the relative displacement of the two potential surfaces (Fig. 13). No calculations for the corresponding local phonon systems are available therefore we use the phonon energies of the Ne matrix for the discussion. Strong and weak coupling are distinguished by the amount of the relative displacement Δ_i of the potential surfaces which can be expressed numerically by the criterion $G \gg 1$ for strong coupling and $G \leq 1$ for weak coupling with

$$13) \quad G \approx E_M/\hbar\langle\omega\rangle$$

For transitions to the ground state the strong coupling limit prevails which is proven by the large Stokes shift (see table 2) between absorption and emission compared to the maximum phonon energy $\hbar\omega_M$ = 7 meV. But within the set of the excited states the relative displacements of the potential curves may be much smaller and the appropriate coupling limit is an open question. Measurements of excited state absorption and emission energies lying in the visible and infrared could answer this question but are not available until now. The temperature dependence for nonradiative transitions from the 5s ($1s_4$) to 5s ($1s_5$) level for Kr atoms in Ar matrix have

been successfully fitted within the weak coupling limit [17]. For a quantitative description the coupling limit has to be clear. We discuss the dependence of the transition rate on the energy spacing ΔE in the weak coupling limit yielding an exponential decrease of the transition rate with increasing ΔE. The energy difference ΔE we take from the separation of the atomic levels. If the strong coupling limit holds we make use of the fact that for given displacements Δ_i, the energy E_A increases monotonically with ΔE. In this case we get a similar strong decrease of the transition rate with increasing ΔE as in the weak coupling limit. This is only true if the changes in relative displacements Δ_i for different states are not too severe. In the strong coupling limit the exponential term will be different because of $E_A < \Delta E$. This has to be kept in mind for the order N of the radiationless transitions in phonon energies $\hbar\omega_M$.

$$14) \qquad N = \frac{\Delta E}{\hbar\omega_M}$$

In the following we take the weak coupling case (equ. 14). As has been explained above for the strong coupling case the order N of the processes has to be reduced to

$$15) \qquad N = \frac{E_A}{\hbar\langle\omega\rangle}$$

Then the energy gap law for the transition rate W can be written as

$$16) \qquad W = W_o \, e^{-\alpha N}$$

Relaxation from n = 2 to n' = 1 and n = 1

Xe in Ne:

After absorption into the n = 2 exciton state the atomic 7s or highest 5d level or both are populated by the matrix relaxation. Relaxation to the 6s' levels takes place within 1 nsec. There are no radiative channels to 6s' which are fast enough. Therefore the relaxation is predominantly nonradiative. Due to the exponential energy gap law (equ. 16) the nonradiative relaxation will go stepwise from one level to the neighbouring level and the transition which has to overcome the largest separation will be the slowest one. Thus this transition determines mainly the total relaxation time. In our case the largest gaps open between the $2s_5$ to $3d_2$ state (Fig. 10) with an energy gap of $\Delta E = 0.161$ eV and from $3d_2$ to $3d_1'$ with an energy gap of $\Delta E = 0.181$ eV. The population will be stored in the $2s_5$ and $3d_2$ state for 1 nsec and in this time radiative decay can compete. We observe a radiative decay time to the ground state of 1.3 nsec which perfectly agrees with the radiative decay time of 1.4 nsec (table 4) of the $3d_2$ state in the free atom. The radiative transition from $2s_5$ is forbidden due to $\Delta J = 2$ and also the transition from the close lying $2s_4$ level will be slower than that from $3d_2$. The order N of the radiationless relaxation processes $2s_5 \rightarrow 3d_2 \rightarrow 3d_1'$ is very large in the weak coupling limit. According to energy gaps $\Delta E \approx 0.18$ eV. the number N of phonons emitted in one step is 16. After passing these two gaps nonradiative relaxation to the 6s' levels will be very fast in the dense manifold of 5d and 6p states.

For Xe/Ne we can go even into more details by using the density dependence of the absorption of Xe atoms dispersed in liquid Ne [23]. The middle part of Fig. 14 shows the change in transition energy as derived from absorption spectra of Xe atoms when the density ρ of the surrounding Ne atoms is increased from ρ = 0 to 0.1, 0.2, 0.4, 0.5 and 0.65 [gcm^{-3}]. In absorption the transitions to $1s_4$, $1s_2$, $3d_5$ ($5d[1/2]$), $3d_2$ ($5d[3/2]$) and $2s_4$ ($7s[3/2]$) are observed which are allowed transitions in the free atom. In addition the transition to $3d_1'$ ($5d[5/2]$) with $\Delta J = 3$ is observed which is induced in the host fluid due to symmetry breaking effects. With increasing Ne density the transitions show characteristic blue shifts as indicated by the connecting lines. On the left hand side of Fig. 14 our excitation spectra for Xe/Ne are reproduced. The positions of the observed maxima are marked at the density of 1.44 [g/cm^{-3}] of solid Ne corresponding to the nearest neighbour separation in solid Ne of 3.2 Å. The maxima due to n = 1 ($1s_4$) and n' = 1 ($1s_2$) states fit smoothly in the trend derived from the density dependence. The maxima lying between n' = 1 and n = 2 are easily identified as the allowed $3d_5$ ($5d[1/2]$) transition and the induced $3d_1'$ ($5d[5/2]$) transition. Messing et al. [23] correlated the n = 2 exciton with $2s_4$ ($7s[3/2]$). Inspecting their Fig. 5 it seems that around densities of 0.4 to 0.5 [g/cm^{-3}] the transition to $2s_4$ ($7s[3/2]$) and $3d_2$ ($5d[3/2]$) merge to one maximum. One can speculate that the following splitting at higher densities is due to a crossing of both levels and perhaps the maximum indicated in Fig. 14 as n = 2 corresponds to $2s_4$ and the next not assigned maximum at higher energies corresponds to $3d_2$ or vice versa. Essential for our discussion will be that the transitions of $3d_2$ and $2s_4$ come close toghether at high densities and are both correlated to the n = 2 exciton. The relaxation of the Ne matrix after excitation of an Xe atom

by the formation of a "bubble" causes a reduced Ne density around the excited Xe atom. The nearest neighbour separation can be regarded as a convenient configuration coordinate. The energies of the excited states will follow the lines in Fig. 14 to lower density i.e. higher nearest neighbour separation. On the righthand side of Fig. 14 our measured emission spectra are reproduced. The positions of the emission bands correspond to nearest neighbour separations of the Xe atom to the surrounding Ne atoms of 3.7 to 5.7 Å as shown by the horizontal and vertical shadowed areas. According to this estimates a bubble is formed with an approximate radius of 4.5 Å corresponding to an increase of the nearest neighbour separation of 1.3 Å or a factor of 1.4. This is a very crude estimate because we place the much larger Xe atoms on a substitutional Ne site. In addition the lattice of the more distant Ne shells causes repulsive forces and an increase in energy at large nearest neighbour separations. These repulsive forces in the solid state are different from the liquid and will modify the energies also at the equilibrium position of the relaxed state. In a recent calculation [24] concerning the bubble formation around excited Ne atoms in pure Ne and considering reorganisation in a cluster up to the 16th shell it was found that the radius of the first shell is increased by a factor of 1.37 and that of the 16th shell still by a factor of 1.011. The close correspondance to our factor is fortuitous, but the general trend seems to be correct.

Finally, the diagram of Fig. 14 explains the radiative and radiationless decay of the n = 2 exciton further. The merging of the $2s_4$ ($7s[3/2]$) and

$3d_2$ ($5d[3/2]$) transition at high density allows a fast relaxation of the n = 2 exciton to $3d_2$ ($5d[3/2]$) which is the lower one at the lower density of the relaxed state. In this way the gap between the $2s_4$ and $3d_2$ state existing in the free atom is bridged. On the other hand the gap between the $3d_2$ ($5d[3/2]$) state and the next lower one $3d_1'$ ($5d[5/2]$) remains constant ($\Delta E \sim 0.2$ eV). Therefore radiationless relaxation will be interrupted at the $3d_2$ state with a time constant of 1 nsec and only radiative decay from $3d_2$ with its radiative decay time of 1.3 nsec is observed. On the right hand side the states with dipole forbidden transitions to the ground state are shown as short horizontal lines. The change of these states with density is not known but when it follows the general trends then the region from $3d_1'$ to $1s_2$ is filled densely with states. Therefore nonradiative relaxation from $3d_1'$ to $1s_2$ will be fast. The large gap between $1s_2$ and $1s_4$ remains.

Kr in Ne:

After n = 2 exciton excitation the $2s_4$ or the $3d_2$ states will be populated by the matrix relaxation (Fig. 11). Due to the high density of lower lying 5 p' and further 4d states the original states are depopulated very fast by radiationless relaxation to the lowest 4d states ($3d_5$, $3d_6$). According to the experiment these processes are so fast that even the very fast radiative decay τ = 1.9 nsec of the $3d_2$ state to the ground state cannot compete. A much longer lifetime of the emitting state is observed. In the lowest 4d states the population will be stored due to the following gap to the 5p states. Indeed the observed radiative lifetime to the ground state of 13 nsec is comparable with the radiative lifetime of the $3d_5$ level of 44.5 nsec in the free atom

which is close to the lowest d level $3d_6$. The gap ΔE between the $3d_6$ state and the highest 5p state $2p_5$ is quite large: ΔE = 0.332 eV and requires in the weak coupling limit an order N = 48.

In the next step the population will be dissipated to the lower 5p states. Three facts determine the further relaxation cascade:

i) after the 5p levels a further even larger gap opens to the 5s' states

ii) quite effective radiative channels to the lower states are possible

iii) due to the symmetry of the states - only 5p states are present, the 5p' lie at higher energies.-radiative relaxation favours very strongly the 5s states compared to the 5s' states.

There are two arguments that the nonradiative channel from the 5p states to the 5s', 5s states is weak. First according to the energy gap law nonradiative relaxation should go stepwise thus via the 5s' state. According to the experiment this state is bypassed. Second the total relaxation time is not faster than the time for the competing radiative channels. The distribution of intensity to the 5s' and 5s states simply follows from the radiative transition rates in the free atoms. For example the transition time from the lower 5p level to the two 5s' states $1s_2$ and $1s_3$ is 30.000 nsec and 20.000 nsec respectively, whereas it is 380 nsec and 45 nsec for the transitions to the two 5s states $1s_4$ and $1s_5$ respectively. The shortest times from the manifold of 5p states to the 5s' states are all longer than 5000 nsec whereas they are 23 and 30 nsec for the $1s_5$ and $1s_4$ component [25]. This decay times agree quite well with the experimental result of 22 nsec for relaxation to each of the two 5s levels ($1s_5$, $1s_4$). The experimental value of 750 nsec for the 5s' levels may contain also the quite weak radiationless contribution to the relaxation

cascade. A distinction if both or only one 5s' level are populated has not been possible due to the low intensity of this emission when higher states are excited.

The description of the relaxation process in this way leads to some problems. First many levels are involved and it would be necessary to evaluate the cascade for all possible radiative and nonradiative transitions by using for example the formalism given by Curtis [26]. Without more information too many free parameters would have to be introduced. An adequate simplification could be, to use one common radiationless transition rate from 4d to the manifold of 5p states and one radiative transition rate from 5p to each of the 5s levels $1s_2$, $1s_3$, $1s_4$ and $1s_5$. In this model each decay curve of one of the 5s levels contains three time constants when n = 2 excitons are populated. The time constants are the radiative decay time of the 5s level to the ground state, the radiative decay time from the 5p to the special 5s level and the nonradiative relaxation rate from 4d to 5p. The time interval of 8 nsec (Fig. 7) for the measurement is too short to attempt a reasonable fit. The same problem will appear for Ar in Ne where the experimental time scale extends to more than 100 nsec. From a comparison with the atomic lifetimes for Kr it seems that the observed relaxation times of 22 nsec and 750 nsec are due to the radiative relaxation from 5p. Radiationless relaxation 4d to 5p is essentially faster.

Ar in Ne:

For Ar in Ne the first steps are quite similar to Kr in Ne. Excitation of n = 2 excitons populates the 3d or 5s states by the fast matrix relaxation. Then fast radiationless relaxation takes place in the close

lying 3d states to the lowest 3d states $3d_5$ and $3d_6$ (Fig. 12). This relaxation is too fast to allow a competition by the radiative decay of the upper 3d level $3d_2$ (τ = 3.7 nsec) or of the 5s level $2s_4$ (τ = 12 nsec). The intensity is stored in the lower 5d states due to the energy gap of ΔE = 0.465 eV between $3d_6$ and the highest 4p' state $2p_1$. The observed radiative lifetime of 420 nsec is attributed to the weak transition from $3d_5$ (or $3d_6$) to the ground state.

Due to the smaller spin orbit splitting of Ar compared to Kr the 4p' and 4p states lie close together. Therefore strong radiative channels from the 4p' to the 4s' and from the 4p to the 4s states are active. Nonradiative channels from the 4p' and 4p states to the 4s states will be weak again because of the large gap and the competing radiative channels. To illustrate the radiative relaxation rates we take the lowest 4p level $2p_{10}$ and the lowest 4p' level $2p_4$. According to Wiese et al. [20] the radiative relaxation rate constants in the free atom from $2p_{10}$ to $1s_2$, $1s_3$, $1s_4$, $1s_5$ are 4000 nsec, 855 nsec, 166 nsec and 47 nsec respectively. From $2p_4$ to $1s_2$, $1s_3$, $1s_4$, and $1s_5$ time constants of 68 nsec, 52 nsec, 4×10^4 nsec and 1500 nsec are obtained. Evidently relaxation from 4p to 4s and from 4p' to 4s' is favoured and the range of the shorter time constants for these transitions is indicated in Fig. 12.

The time constants for the branching to $1s_4$ and $1s_5$ as well as for $1s_2$ and $1s_3$ are determined from the ratio of the areas of the decay curves and the areas of the background. Therefore they are less accurate. With this restriction in mind the agreement of the observed time constants from n = 2 to the 4s and 4s' states with the atomic radiative decay time from 4p and 4p' to 4s and 4s' is quite convincing. On the other hand we

run into the same problem as for Kr in Ne. Our description involves even in the simplest version a cascade of radiationless transitions 3d to 4p and radiative decays from 4p to 4s and from 4s to the ground state. Thus it requires at least three time constants for the decay of the 4s state after n = 2 exciton population. The same is true for the cascade 3d → 4p' → 4s' → ground state. When a set of three times is used for each emission band I and II after n = 2 excitation then two times are approximately fixed by the radiative decay times of the 4s, 4s' states to the ground state (which are known from n = 1 and n' = 1 excitation) and also the depopulation time of the 3d states is known from emission band III. Under these conditions a reasonable fit of each of the decay curves (Ic and IIe Fig. 8) with three time constants requires radiationless relaxation times from 3d to 4p and from 3d to 4p' which are shorter than 5 nsec. This is in contrast to the total lifetime of the 3d states of 13 nsec given by the decay of emission band III. As long as further experimental observations as for example the investigation of the emission 4p → 4s are missing we can only speculate. In the matrix shifts of the states perhaps reduce the separation between 4p and 3d states causing fast nonradiative relaxation to the 4p', 4p states. Also breaking of the selection rules perhaps allows emission with a radiative lifetime of 420 nsec from the mixture of 4p and 3d states.

Intersystem crossing: n' = 1 → n = 1

For the relaxation from n = 2 to n = 1 the nonradiative relaxation has been discussed only in terms of the energy gaps and selection rules have been neglected, whereas for the radiative part of relaxation selection rules

determined the atomic transition probabilities. Due to the close lying manifold of states of different symmetry involved in the radiationless transitions selection rules may be washed or do not shine up separately in the experiment. The situation is different for the relaxation of n' = 1 to n = 1. Due to absorption in n' = 1 and matrix relaxation the $1s_2$ state i.e. the $^1P_1$ states of Xe, Kr and Ar guest atoms are populated. The scheme of Fig. 15 shows that three well defined states lie below the primarily populated $^1P_1$ state and the possible transitions are indicated by the arrows 1 to 6. The picture is even more complicated because the lower states of Xe show an additional splitting attributed to a site symmetry splitting [14]. For the discussion we restrict ourselves to the scheme of Fig. 15. From the experimental observations it follows immediately that the ^3P_o and the $^3P_2$ states do not emit when either n = 1 or n' = 1 excitons are populated by light. This means channel (2) to (6) are omitted by the radiationless relaxation processes. Selection rules explain this observation. For $^1P_1 \rightarrow {}^3P_o$ the forbiddeness of J = 1 to J = o transition in radiationless processes has to be broken and further it would be an intersystem crossing transition S = 1 to S = 3. For Kr / Ar the transition $^3P_1 \rightarrow {}^3P_2$ has been observed [17], but in the Ne matrix evidently the change of J = 1 to J = 2 is not probable enough. Finally the experimental time constants show if intersystem crossing from $^1P_1$ to $^3P_1$ takes place in the series of guest atoms. Following the energy gap law the transition probability is determined by the electronic matrix element and the energy gap. The matrix element W_o for intersystem crossing is given mainly by the spin orbit coupling strength. An increasing spin orbit coupling strength causes larger preexponential factors W_o but on the other hand due to the also increasing energy gap the exponential term in the radiationless transi-

tion rate decreases (equ. 16). The heavy rare gas atom Xe shows the strongest spin orbit coupling with an energy gap ΔE of 1.2 eV (table 2). The very large gap would require radiationless processes of the order N = 170. Even the largest preexponential factor expected in this series cannot compensate the very small exponential term.

For the lightest atom Ar with the smaller spin orbit coupling strength the splitting ΔE is only 0.22 eV corresponding to a transition of the order N = 30. But according to the experiment the preexponential factor is too small to allow a radiationless transition faster than 100 nsec.

For Kr with a splitting of 0.68 eV both competing factors could allow the radiationless transition. Again the relaxation is slow, at least slower than 1.9 nsec and probably it even has not been observed.

6. Comparison with emission spectra at higher resolution.

Schuberth and Creuzburg [14] published emission spectra of Xe, Kr and Ar atoms in bulk polycrystals of Ne excited by x-rays. The resolution was better than the linewidth of the emission bands. The concentration dependence concerning the intensities of monomer and dimer emissions from guest atoms and the intensities of impurity emission are different from our results. In the bulk crystals monomer emission dominates the spectra only at concentrations less than 20 ppm. The dimer luminescence increased in going from 5 to 50 ppm. At higher concentrations also the dimer intensity decreased and impurity emission was observed. In our experiments no impurity bands have been observed. The monomer emission dominated up to 5000 ppm. For concentrations of the order of 1 % dimer

emission became strong. The intensities of the bands did not depend on time after preparation or illumination time. We attribute the differences to special clustering problems during crystal growth and to the migration of the excitation energy in the crystal due to the high energetic excitation.

Fig. 16 shows a comparison of the emission spectra of Schuberth and Creuzburg [14] and our emission spectra. The significant differences are first the splitting of bands I and II due to the higher resolution and second the absence of the bands III in the spectra of Schuberth et al. The excitation spectra and tests with atmospheric gases proofed that the bands III are inherent to the guest atoms and not due to impurities. It is not yet clear why they have not been observed by Schuberth et al. In our opinion, the splitting should be attributed to the fine structure components $1s_2$, $1s_3$, $1s_4$, $1s_5$ which are blue shifted due to the surroundings as discussed in detail for Xe in Ne before. Except for Xe, the splittings are quite similar to the atomic ones. Our results showed that for excitation energies larger than the energies of the n = 2 excitons a short living and a long living component are contained in each of the bands I and II. The long living parts are due to the decay of $1s_3$ (^3P_o) and $1s_5$ ($^3P_2$) states which are strictly forbidden in the free atom but are weakly induced by the matrix. The short living parts from $1s_2$ ($^1P_1$) and $1s_4$ ($^3P_1$) are both strongly allowed. The appearance of three components in band I of Xe may be caused by an additional splitting of the $^3P_2$ state into Γ_3^- and Γ_5^- states as expected in the O_h symmetry of the matrix fcc lattice.

We believe in contrast to the arguments of Schuberth et al. that we can explain the observed intensities of the bands by the population channels using our results for the relaxation cascades. As we have shown no relaxation happens between the states $1s_2$, $1s_3$, $1s_4$ and $1s_5$ except perhaps for the transition $1s_2 \rightarrow 1s_4$ in Kr. Therefore the states decay independently and the intensities of these bands (with the one exception) are not influenced by the lifetime of these states (short or long) but are only determined by the population rates. We consider as the main population channel after X-ray excitation energy transfer of free and relaxed Ne exciton states. The transferred energies lie in the region from 14 eV to 20 eV, thus, corresponding to regions in our excitation spectra above the n = 2 excitons of the guest atoms. As weak channels we expect direct absorption of X-rays at the guest atoms and excitation of the guest atoms by electron energy loss processes due to high energetic electrons which are created after X-ray excitation of the host.

Xe in Ne:

The dominant excitation channel will be energy transfer from the Ne host with energies larger than 14 eV, subsequent fast relaxation to n = 2 or the corresponding 7s and 5d states and then within 1 nsec nonradiative relaxation exclusively to $1s_2$ takes place. Therefore most of the emission is concentrated in the single $1s_2$ band. The very weak population of $1s_4$ and $1s_5$ is attributed to electron energy loss processes which will also create n = 1 excitons of the guest atoms. In energy loss processes of low energetic electrons the dipol selection rules are not active and also the dipol forbidden $^3P_2$ state ($1s_5$) will be populated.

Kr in Ne:

Again energy transfer with subsequent relaxation in the guest atomic like states will be the main excitation source. But in Kr the relaxation is radiatively. As has been discussed this radiative decay favours strongly transitions to $1s_4$ ($^3P_1$) and $1s_5$ ($^3P_2$) which according to our results are populated with equal probability. An error of 50 % (Schuberth et al. observe a ratio I ($1s_4$) : I (s_5) = 1:2) seems somewhat large, but cannot be excluded. The weak emission from $1s_2$ and $1s_3$ expected from our results can be suppressed in the crystal by stronger reabsorption after X-ray excitation with large penetration depth.

Ar in Ne:

Again after energy transfer and nonradiative relaxation the radiative relaxation from 4p' and 4p to 4s' and 4s will determine the intensity distribution. From our relaxation times an intensity of $1s_2$: $1s_3$: $1s_4$: $1s_5$ = 45 : 39 : 50 : 100 is derived which fits within our accuracy quite well to the ratio 30 : 10 : 30 : 100 observed by Schuberth et al.

7. Summary

From excitation spectra, emission spectra and decay curves of Xe, Kr and Ar guest atoms in solid Ne matrix information concerning the primarily excited states, the emitting states and the time dependence of the relaxation processes between these states has been derived.

1) The primarily excited states of heavier rare gas guest atoms in Ne matrix are attributed to two series of Wannier type atomic impurity states, which are separated by the spin orbit splitting of the guest atoms. In addition, blue shifted 5d states of Xe atoms are observed

for Xe in Ne.

2) After excitation a cavity is formed around the excited guest atoms by a very fast relaxation ($\tau < 10^{-11}$ sec.) of the surrounding Ne atoms. In the cavity the nearest neighbour separation is 1 Å - 2 Å larger than in the ground state configuration.

3) In emission three bands are observed for each species of guest atoms which belong to transitions from ns, ns' and (n-1)d states to the ground state. The emission energies lie between the excitation energies in the matrix and the energies of the free atomic transitions. The radiative lifetimes of the states in the matrix are very similar to the free atomic lifetimes of the corresponding states.

4) Radiative or nonradiative relaxation has not been observed between the fine structure components $1s_2$, $1s_3$, $1s_4$, $1s_5$ ($^1P_1$, $^3P_0$, $^3P_1$, $^3P_2$) on a time scale of some hundred nanoseconds except perhaps the $1s_2$ - $1s_4$ transition in Kr.

5) For Kr a strong resonant energy transfer from the relaxed $1s_2$ state to the unrelaxed n = 1 state of a neighbouring Kr atom causing finally a $1s_2$ - $1s_4$ transition has been observed.

6) The relaxation channels from n = 2 exciton states to the lower lying states are different for Xe, Kr and Ar. In Xe pure nonradiative relaxation on a nsec time scale from 5d states to the 6s' state obeying an energy gap law has been observed. In Kr and Ar the relaxation times of the order of 10 to 1000 nsec are mainly determined by radiative

relaxation from 5p and 4p, 4p' states to the ns and ns' states respectively.

7) The radiative relaxation channels in Kr and Ar also populate the metastable $1s_5$ ($^3P_2$) and $1s_3$ ($^3P_0$) levels. The radiative decay of the metastable states exceeds our range of 1 µsec. Using our population efficiencies the intensity distribution in highly resolved emission spectra after X-ray excitation can be explained.

Acknowledgement

We would like to acknowledge the experimental support by Prof. R. Haensel and Prof. G. Zimmerer.
We also acknowledge the discussions by Dr. V. Saile who has carefully read this manuscript.
This work has been supported in part by Bundesministerium für Forschung und Technologie BMFT from funds for Synchrotron Radiation Research.

Appendix:

The experimental time response function R (t) is determined by measuring the decay curve for reflected light which is prompt. The response function has a fwhm of 400 psec which contains the width of the excitation pulse, the jitter of the channel plate (∿ 50 psec) and time distortions due to the electronics. From the measured time dependence I (t) of the luminescence intensity rise times and decay times of emission have to be extracted. The real time dependence F (t) of emission is separated from the experimental broadening due to the response function R (t) by calculating F (t) from the convolution:

$$I(t) = \int_0^t R(t)\ F(t - t')\ dt$$

For R (t) the numerical values and also an approximation by

$$R(t) = A \exp\left\{(t-t'_o)^2/2\sigma^2\right\}$$

with σ = 250 psec have been used. The analysis shows that for rise and decay times contained in F (t) longer than 1 nsec the contribution of R (t) can be neglected. These time constants are derived directly from I (t). With the convolution values for time constants down to 50 psec have been determined and a lower limit of 10 psec is detectable. Due to the repetition rate of at least 1 MHz of the light pulses, time constants longer than 1 µsec cause a more or less constant background. From the height of the background the appearance of long decay times and the branching ratios relative to the shorter components have been derived, but not quantative time constants.

F (t) consists of a sum of positive and negative exponential functions $A_i \exp(-t/\tau_i)$. In the following the index i stands for the initial state and the index j for the final state of the relaxation transitions. The short time constants τ_i cause a negative preexponential factor A_i and correspond to rise times in F (t). The longer time constants have a positive A_i and correspond to decay times. The number m' of possible time constants is determined by the number m of levels contributing to the relaxation cascade investigated and amounts to $m' = \frac{m}{2}(m-1)$. A cascade of three primarily excited electronic states n = 1, n' = 1 and n = 2 and three Stoke's shifted emitting states consists of at least 7 levels including the ground state (Fig. 17a).

The equations to extract the time constants τ_{ij} for transitions from level i to level j for a 5 level system are given below, using the experimental rise and decay times τ_i and intensities F_i of the emission bands. n_i (t) corresponds to the time dependence of the population of level i with total lifetime τ_i after δpulse excitation. The arrangement of the levels allows to take the same equations also for a system with less levels by ignoring the higher indexes.

$$n_1(t) = \exp(-t/\tau_1)$$

$$n_2(t) = \frac{\tau_1 \cdot \tau_2}{(\tau_2 - \tau_1) \cdot \tau_{12}} \cdot \{\exp(-t/\tau_2) - \exp(-t/\tau_1)\}$$

$$n_3(t) = C_1\{\exp(-t/\tau_1) - \exp(-t/\tau_3) - C_2\{\exp(-t/\tau_2) - \exp(-t/\tau_3)\}$$

$$C_1 = \frac{R_{13}}{\tau_{13}} + \frac{R_{12} \cdot R_{13}}{\tau_{12} \cdot \tau_{23}} \quad ; \quad C_2 = \frac{R_{12} \cdot R_{23}}{\tau_{12} \cdot \tau_{23}}$$

$$n_4(t) = D_1(\exp(-t/\tau_1) - \exp(-t/\tau_4)\} - D_2\{\exp(-t/\tau_2) - \exp(-t/\tau_4)\} + D_3\{\exp(-t/\tau_3) - \exp(-t/\tau_4)\}$$

$$D_1 = R_{14}\left(\frac{1}{\tau_{14}} + \frac{R_{12}}{\tau_{24} \cdot \tau_{12}} + \frac{C_1}{\tau_{34}}\right)$$

$$D_2 = R_{24}\left(\frac{R_{12}}{\tau_{24} \cdot \tau_{12}} - \frac{C_2}{\tau_{34}}\right)$$

$$D_3 = \frac{R_{34}}{\tau_{34}}(C_2 - C_1)$$

with $R_{ij} = \frac{\tau_i \tau_j}{\tau_i - \tau_j}$

The time dependence of the luminescence intensity I_i from level i follows from

$$I_i = \frac{n_i(t)}{\tau_{io}}$$

The total luminescence intensity F_i for transition from level i to the ground state is given by:

$$F_i = \frac{1}{\tau_{io}} \int_0^\infty n_i(t)dt$$

$$F_1 = \frac{\tau_1}{\tau_{10}}$$

$$F_2 = \frac{\tau_1 \cdot \tau_2}{\tau_{12} \cdot \tau_{20}}$$

$$F_3 = \frac{\tau_1}{\tau_{30}}\left(\frac{\tau_3}{\tau_{13}} + \frac{\tau_3 \cdot \tau_2}{\tau_{12} \cdot \tau_{23}}\right)$$

$$F_4 = \frac{1}{\tau_{40}}\left(D_1(\tau_1 - \tau_4) - D_2(\tau_2 - \tau_4) + D_3(\tau_3 - \tau_4)\right)$$

According to the experimental results the relaxation causing the stokes shift (matrix relaxation) is much faster than all other time constants and the cascade can be simplified to a four level system (Fig. 17b). Therefore the expression for explicit time constants are given here only for a four level scheme.

$$\tau_{20} = \tau_2\left(1 + \frac{\tau_2}{F_{23}(\tau_2 + A_3)}\right)$$

$$\tau_{23} = \tau_2 + F_{23}(\tau_2 + A_3)$$

$$\tau_{12} = \tau_1\left(\frac{(1 + F_{23}(1 + F_{12}))(A_3 + \tau_2)}{\tau_2 + F_{23}(A_3 + \tau_2)}\right)$$

$$\tau_{13} = \tau_{12} \cdot \frac{\tau_{23}}{A_3}$$

$$\tau_{10} = \tau_1\left(\frac{1}{1 - \frac{\tau_1}{\tau_{12}}(1 + \frac{A_3}{\tau_{23}})}\right)$$

with

$$A_3 = R_{12}\frac{R_{23}}{R_{13}}C_{12} - R_{12}$$

$$C_{12} = C_1 / C_2$$

$$F_{12} = F_1 / F_2$$

$$F_{23} = F_2 / F_3$$

On the other hand the emission from the n = 1 and n' = 1 excitons contains two components, but only for excitation to states above n' = 1. This shows that two different states contribute to each of these emission bands. The experimental results indicate that no relaxation takes place between the two subcomponents of the n = 1 and n' = 1 emission bands. For this cascade total relaxation times τ_{13} and τ_{12} are derived from the four level system. The branching ratio of the relaxation times to the sublevels s_2, s_3, s_4, s_5 (Fig. 17 c) simply follows from the intensities I_{s_5}, I_{s_4} contained in emission from n = 1 and I_{s_2}, I_{s_3} for emission from n'= 1.

$$\tau_{1s_5} = (1+I_{s_4}/I_{s_5})\tau_{13}; \qquad \tau_{1s_4} = (1+I_{s_5}/I_{s_4})\tau_{13}$$

$$\tau_{1s_3} = (1+I_{s_2}/I_{s_3})\tau_{12}; \qquad \tau_{1s_2} = (1+I_{s_3}/I_{s_2})\tau_{12}$$

The evaluation of all experimental data has been started on the basis of the four level system including the sublevels. A fit of a decay curve with a free variation of 3 time constants τ_i and 3 factors A_i would be quite doubtful. Therefore in the evalution we build up the cascade by solving the much simpler problem for direct population of the n = 1 exciton. Then we go on stepwise to the higher states using the previously determined time constants of the lower states. Finally we check the consistency by introducing all time constants and experimental results in the general equations. In most cases the evalution showed that the equations for a three level system including sublevels are sufficient to describe the decay curves because only very few decay channels are really active.

References

1) "Rare Gas Solids" ed. M.L. Klein and J.A. Venables, Academic Press Vol. I (1976), Vol. II (1978), Vol. III in preparation

2) B. Sonntag in ref. 1, chapter 19

3) a) J. Jortner in "Vacuum Ultraviolet Radiation Physics", ed. E.E. Koch, R. Haensel and C. Kunz, Pergamon-Vieweg, Braunschweig (1974)
b) G. Zimmerer in "Luminescence of Inorganic Solids", ed. B. DiBartolo and D. Pacheco, Plenum Press, 1978, p. 645
c) N. Schwentner in "Luminescence of Inorganic Solids", ed. B. DiBartolo and D. Pacheco, Plenum Press, 1978, p. 645-665
d) I.Ya. Fugol, Advances in Physics 27 (1978) 1

4) N. Schwentner and E.E. Koch, Phys. Rev. B 14 (1976) 4687

5) R. Reisfeld in "Structure and Bonding" Vol. 22 eds. J.O. Dunitz, P. Hemmerich, R.H. Holm, J.A. Ibers, C.Ic. Jørgensen, J.B. Neilands, D. Reiners, R.J.P. Williams, Springer, Berlin-Heidelberg-New York (1975)

6) R. Brodman, U. Hahn and G. Zimmerer, Chem. Phys. Lett. 41 (1976) 160

7) U. Hahn, N. Schwentner and G. Zimmerer, Nucl. Instr. and Methods 152 (1978), 261

8) S. Cova, M. Bertolaccini, C. Bussolati, Phys. Stat. Sol. (a) 18 (1973) 11

9) G. Baldini, Phys. Rev. 137 (1965) 508

10) D. Pudewill, F.-J. Himpsel, V. Saile, N. Schwentner, M. Skibowski and E.E. Koch, phys. stat. sol. (b) 74 (1976) 485

11) V. Saile and E.E. Koch, Phys. Rev. B 20 (1979) 784

12) A. Gedanken, B. Raz and J. Jortner, J. Chem. Phys. 59 (1973) 5471

13) I.Ya. Fugol, Advances in Physics 27 (1978) 1

14) E. Schuberth and M. Creuzburg, Phys. Stat. Sol. 90 (1978) 1

15) W.B. Person, J. Chem. Phys. 28 (1958) 319

16) H. Dubost, R. Charnean, Chem. Phys. 12 (1976) 407

17) U. Hahn, R. Haensel, N. Schwentner and G. Zimmerer, to be published

18) Z. Ophir, M. Sc. Thesis, Tel-Aviv (1970)

19) C.E. Moore "Atomic Energy Levels", Vol. I, II, III, U.S. Department of Comm., NBS 467 (1949, 1952, 1958)

20) W.L. Wiese, M.W. Smith, B.M. Miles in "Atomic Transition Probabilities II (Na-Ca)" 192 (1969) NSRDS-NBS 22

21) F. Auzel in "Luminescence of Inorganic Solids" ed. B. DiBartolo and D. Pacheco, Plenum Press, 1978 p

22) R. Englman and J. Jortner, Mol. Phys. 18 (1970) 145

23) I. Messing, B. Raz and J. Jortner, submitted to Chem. Phys.

24) P.L. Kunsch and F. Coletti, J. Chem. Phys. 70 (1979) 726

25) R.A. Lilly, J.O.S.A. 66 (1976) 245

26) S.M. Younger and W.L. Wiese, Phys. Rev. 17 (1978) 1944

table 1:

Maxima in the excitation spectra of emission bands I,II and III are correlated with exciton states and compared with absorption spectra and with calculated exciton energies (equ. 4). Energies in eV.

table 2:

Position of emission bands (E) and comparison with the corresponding states in absorption (A) and in the free atom (G). Energies in eV.

table 3:

Experimental rise times τ_1, decay times τ_2, intensity ratios F between long background and fast components and relativ intensities R of emission bands I, II and III at the excitation energies a, b, c. Times in nanoseconds.

table 4:

Radiative lifetimes in the Ne matrix and in the free atom. For comparison also values corrected for the index of refraction of the matrix (see text). Times in nanoseconds.

table 5:

Experimental relaxation times between excited guest atom states in Ne matrix. Times in nanoseconds.

Figure captions:

1) Top: scheme of the experimental arrangement;
MP: primary monochromator; FS: focusing mirror;
P: sample holder; L: luminescence light; MS: secondary monochromator;
PM: photomultiplier; VK: cryostat; GE: gas inlet tube.
Bottom: scheme of the time resolving electronics;
DORIS: storage ring; BT: bunch trigger; DL: delay line;
CD: constant fraction discriminator; TAC: time to amplitude converter;
ADC: analog to digital converter; MC: multichannel analyser;
PL: plotter.

2) Emission spectra for Xe, Kr and Ar atoms in Ne matrix with emission bands I, II and III. The atomic states are also shown. Long bars correspond to dipole allowed transitions and short bars to forbidden transitions to the ground state. The absolute position of the atomic transitions have been shifted by 0.23 eV for Xe, 0.14 eV for Kr and 0.09 eV for Ar to the blue to get coincidence of emission band II and the allowed 6s' transition.

3) Excitation spectra (emission intensity versus excitation energy) of Xe in Ne (hatched curves) for each of the three emission bands I, II and III. Each emission band is shown in front of the corresponding excitation spectrum on the same energy scale. Prominent maxima in the excitation spectra are marked by a,b,c,d,e (see text). Further the positions of excitonic states n = 1,2,3,4 and n = 1', 2', 3', 4' are shown. The inserts at the right hand side provide a survey about the

time dependence of the intensity in the emission bands at prominent excitation energies (see also Fig. 6). The left hand side insert shows the complete emission spectrum.

4) Excitation spectrum for Kr in Ne similar to Fig. 3.

5) Excitation spectrum for Ar in Ne similar to Fig. 3.

6) Decay curves for Xe in Ne in the emission bands ($\hbar\omega_{em}$) I,II and III at the excitation energies ($\hbar\omega_{ex}$) a,b,c from Fig. 3. The fits result from a three level scheme with the lifetimes τ_1 and τ_2 of the upper and lower level. A background with the intensity ratio F compared to the fast components is included (see table 3).

7) Decay curves for Kr in Ne like Fig. 6. For the exception of curve Ib see text.

8) Decay curves of Ar in Ne like Fig. 6.

9) Energy level scheme for the Ne host and the Xe, Kr and Ar guest states. B is the exciton binding energy calculated from excitons $n \geq 2$.

10) Left hand side: Experimental radiative (⇝) and nonradiative (⟶) electronic relaxation pathways and time constants (in nanoseconds) for Xe/Ne in a configuration coordinate diagram. The excitation channels n = 1, n' = 1 and n = 2 and the matrix relaxation (⇝) are included.

Right hand side: atomic energy levels (Paschen notation) of Xe with some lifetimes for radiative transitions to the ground state (~~~). Long bars correspond to states with allowed, short bars to forbidden transitions to the ground state.

11) Relaxation cascade for Kr in Ne like Fig. 10. Important radiative transitions between excited atomic transitions are included (≈≈).

12) Relaxations cascade for Ar in Ne like Fig's 10 and 11.

13) Configuration coordinate scheme for radiationless transitions in the weak (a) and strong (b) coupling limit.

14) Dependence of the energy position of the lowest states of Xe atoms on the density of surrounding Ne atoms (ref. 23). The density is expressed by the mean nearest neighbour separation between a Xe atom and surrounding Ne atoms. The Ne density ranges from 0 through liquid and solid phase. For the solid Ne phase (density 1,44 $[g\ cm^{-3}]$ $\hat{=}$ 3.13 Å)the maxima of our excitation spectra (left hand side) have been included. The density around relaxed Xe atoms follows from a comparison with our emission spectra (right hand side, horizontal lines).

15) Scheme of the lowest excited states for rare gas atoms, showing the 6 possible relaxation channels.

16) Comparison of the high resolution emission spectra of Schuberth and Creuzburg [14] (upper curves) with our spectra (lower curves).

17) a) Pathway for excitation and relaxation in a 7 level system. 0,1,3,5: primarily excited states; 2,4,6: states after matrix relaxation.

b) Nomenclature for the case of a very fast matrix relaxation compared to other time constants. 4 level scheme: 0,1,2,3.

c) Nomenclature for a similar system including two additional sublevels s_3, s_5. Relaxation between the levels s_2, s_3, s_4, s_5 does not take place. s_2, s_3, s_4, s_5 correspond to the fine structure components of the rare gas atoms according to the notation of Paschen.

	emission bands in Ne matrix (E) this work		ref.12	ref.14	atomic levels (G)		absorption bands in Ne matrix (A)		(A)-(E)	(G)-(E)
Xe			8.43	8.34;8.47	$6s\{^{1s_5}_{1s_4}$	8.31				
	I	8.61	-	8.61		8.44	n = 1	9.06	0.45	- 0.17
	II	9.80	9.56	9.77	$6s'_1s_2$	9.57	n = 1'	10.05	0.25	- 0.23
0.01 %	III	10.78	-	-	$5d,3d_2$	10.40	n = 2	11.32	0.54	- 0.38
Kr			10.03	10.02	$5s\{^{1s_5}_{1s_4}$	9.91				
	I	10.10	-	10.16		10.03	n = 1	10.60	0.5	- 0.07
	II	10.78	-	-	$5s'_1s_2$	10.64	n = 1'	11.22	0.44	- 0.14
0.01 %	III	12.12	-	-	$4d,3d_5$	12.04	n = 2	13.35	1.23	- 0.08
Ar			11.61	11.63	$4s\{^{1s_5}_{1s_4}$	11.54				
	I	11.70	-	11.71		11.62	n = 1	12.51	0.81	- 0.08
				11.81	$4s'\{^{1s_3}_{1s_2}$	11.72				
	II	11.92	-	11.92		11.83	n = 1	12.74	0.82	- 0.09
0.3 %	III	13.93	-	-	$3d,3d_5$	13.86	n = 2	14.82	0.89	- 0.07

table 2

	excitation energy I	II	III	exciton	absorption ref.10	ref.9	calculated energies
Xe/Ne	9.1	-		n = 1	9.06	9.08	
		10.06		n = 1'	10.05	10.04	
		10.35					
		10.95					
		11.31	11.32	n = 2	11.32	11.28	11.32
		11.53	11.53				
		-	11.75				
		11.84	11.83				
		11.99	12.01	n = 3			12.01
		12.18	12.20	n = 4			12.26
		-	12.43	n = 5			12.39
		12.62	12.57	n = 2'	12.59		12.59
		12.81	12.86				
		13.35	13.33	n = 3'	13.32		13.28
Kr/Ne	10.6			n = 1	10.68	10.62	
	10.85						
	11.20	11.22		n = 1'	11.29	11.22	
		11.54					
	13.12	13.12					
	13.32	13.32	13.34	n = 2	13.45		13.32
	13.90	13.98	13.94	n = 2'	14.06		13.95
	14.04		14.06	n = 3	14.14		14.01
	14.18			n = 4			14.26
	14.48		14.48	n = 3'	14.55		14.64
Ar/Ne	12.48	(12.37)		n = 1	12.59	12.5	
	(12.74)	12.74		n = 1'	12.80	12.7	
	14.84	14.84	14.84	n = 2	14.97		14.84
	15.02	15.00	15.00				
	15.16	15.18	15.1				
	15.24	15.25	15.26	n = 2'	15.31		15.25
	15.49	15.53	15.52	n = 3	15.67		15.51
	15.75	15.75	15.73	n = 4	15.90		15.75
	15.94		15.80	n = 3'	16.04		15.94

table 1

		radiative lifetime in Ne matrix	correction factor	corrected values	atomic radiative lifetimes
Xe	$6s, 1s_4$	2.4 ± 0.2		2.93 (2.66)	3.46 ± 0.09 [a]
	$6s, 1s_2$	3.5 ± 0.2		4.27 (3.88)	3.44 ± 0.07 [a]
	$5d, 3d_2$	1.3 ± 0.2	1.22 (1.11)	1.59 (1.44)	1.40 ± 0.07 [a]
Kr	$5s, 1s_4$	2.5 ± 0.2		2.92 (2.78)	3.18 ± 0.12 [a]
	$5s', 1s_2$	3.1 ± 0.5	1.17 (1.11)	3.63 (3.44)	3.11 ± 0.12 [a]
	$4d, 3d_5$	13.0 ± 2		15.2 (14.4)	44.5 [b]
Ar	$4s, 1s_4$	5.8 ± 0.3		6.61 (6.43)	8.4 [c]
	$4s', 1s_2$	1.2 ± 0.2	1.14 (1.11)	1.37 (1.22)	2.0 [c]
	$3d, 3d_5$	420 ± 20		4.80 (4.66)	?

table 4

a) E. Matthias, R.A. Rosenberg, E.D. Poliakoff, M.G. White, S.-T. Lee and D.A. Shirley, submitted to Chem. Phys. Letters 52, 239 (1977)

b) P.F. Gruzdev and A.V. Loginov
Opt. Spectrosc. 38 (1975) 611

c) W.L. Wiese, M.W. Smith, B.M. Miles,
in "Atomic Transition Probabilities II (Na-Ca)"
192 (1969) NSRDS - NBS 22

a : n = 1 b : n' = 1 c : n = 2

	emission band	τ_1	τ_2	F	R	τ_1	τ_2	F	R	τ_1	τ_2	F	R
Xe	I	≤ 0.01	$2.4^{+}_{-}0.2$	0	1	-	-	-	0	-	-	-	0
	II	-	-	-	0	≤ 0.01	$3.5^{+}_{-}0.1$	0	1	0.4	$3.7^{+}_{-}0.2$	0	100
	III	-	-	-	0	-	-	-	0	≤ 0.01	0.57	<0.02	69
Kr	I	≤ 0.01	2.5	0	1	$1.2^{+}_{-}0.1$	2.5	0	13.1	2.5	6	1:1	100
	II	-	-	-	0	≤ 0.01	1.2	0	8.1	not measured		-	2.5
	III	-	-	-	0	-	-	-	0	≤ 0.01	6	0	83
Ar	I	≤ 0.01	$5.5^{+}_{-}1$	0	1	-	-	-	≤ 1	$4.0^{+}_{-}1$	$12.6^{+}_{-}0.5$	2:1	100
	II	-	-	-	0	≤ 0.01	$1.2^{+}_{-}0.1$	0	100	$1.2^{+}_{-}0.1$	$12.6^{+}_{-}0.5$	0.86:1	56
	III	-	-	-	0	-	-	0	0	≤ 0.01	$12.6^{+}_{-}0.5$	0	5

table 3

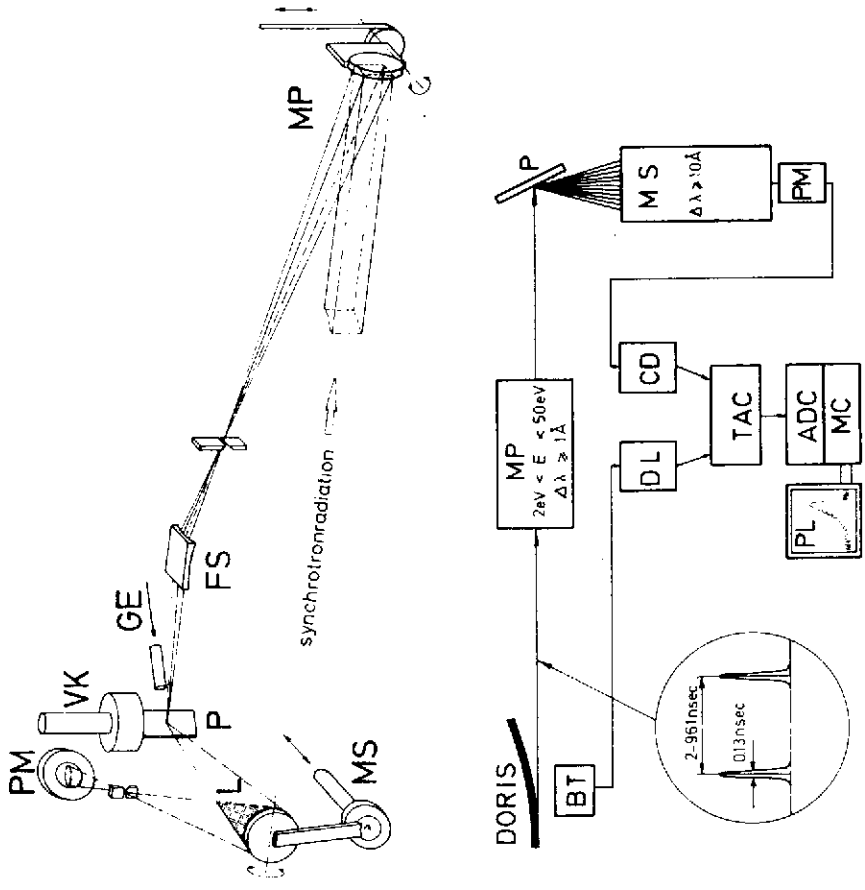

Fig. 1

	$n=2 \rightarrow 1s_2$	$n=2 \rightarrow 1s_3$	$n=2 \rightarrow 1s_4$	$n=2 \rightarrow 1s_5$	$1s_2 \rightarrow 1s_3, 1s_4, 1s_5$	$1s_3 \rightarrow 1s_4, 1s_5$	$1s_4 \rightarrow 1s_5$
Xe	1.0	n.o.	n.o.	n.o.	n.o.	n.o.	n.o
Kr	750	?	22	22	n.o.	n.o.	n.o.
Ar	71	82	63	32	n.o.	n.o.	n.o.

n.o. means: not observed; lower limit $\tau \geq 100$ nsec

table 5

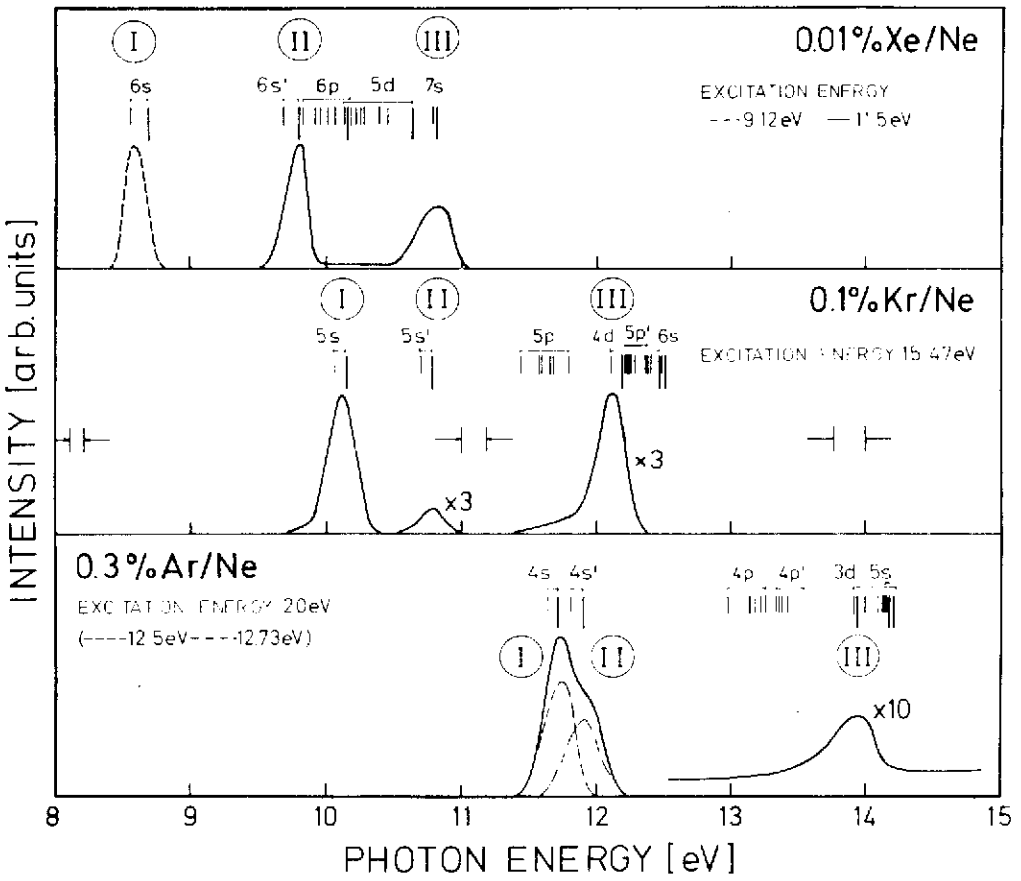
0.01%Xe/Ne
EXCITATION ENERGY
---9.12eV —1'.5eV
6s
6s'
6p
5d
7s
0.1%Kr/Ne
EXCITATION ENERGY 15.47eV
5s
5s'
5p
4d
5p'
6s
×3
×3
0.3%Ar/Ne
EXCITATION ENERGY 20eV
(----12.5eV---12.73eV)
4s
4s'
4p
4p'
3d
5s
×10
INTENSITY [arb.units]
PHOTON ENERGY [eV]

Fig. 2

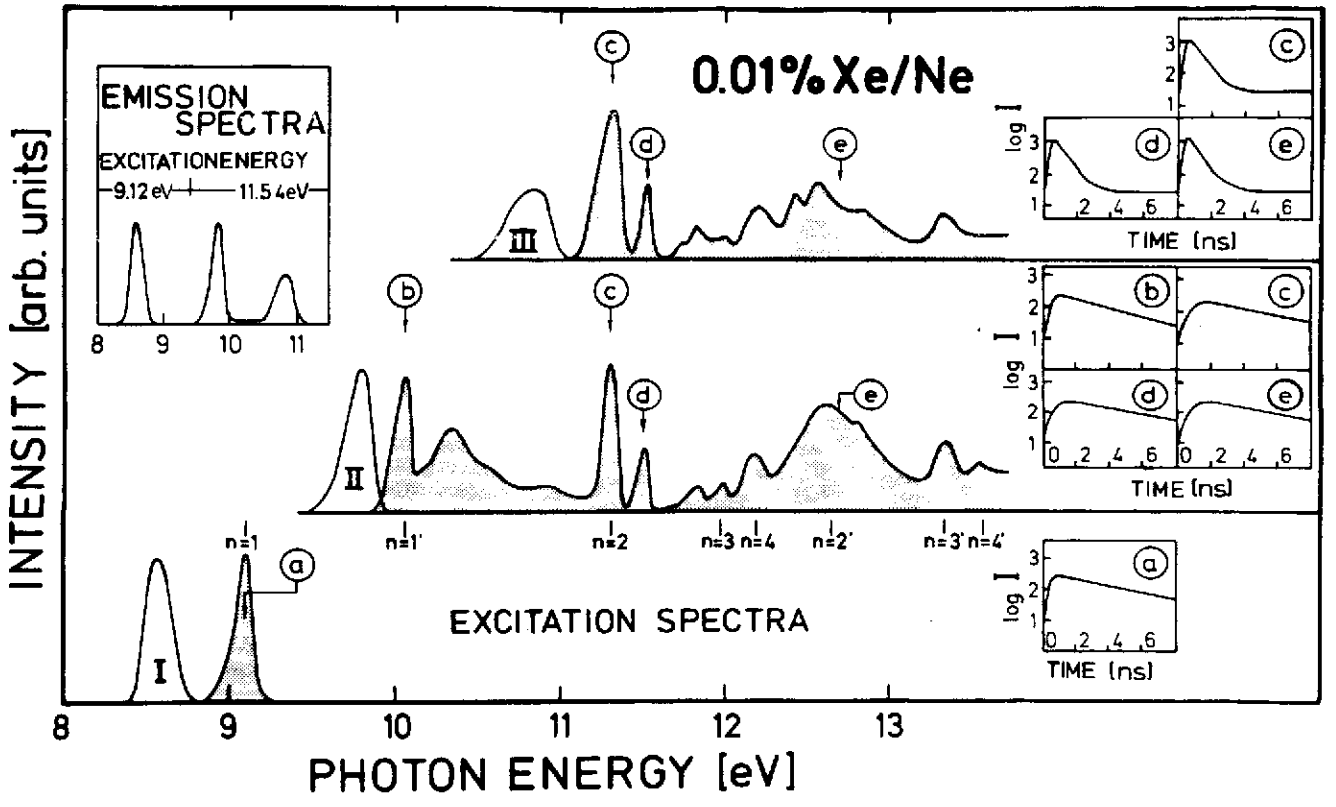
EMISSION SPECTRA
EXCITATIONENERGY
9.12eV
11.54eV
0.01%Xe/Ne
TIME (ns)
TIME (ns)
TIME (ns)
n=1
n=1'
n=2
n=3 n=4
n=2'
n=3' n=4'
EXCITATION SPECTRA
INTENSITY [arb. units]
PHOTON ENERGY [eV]

Fig. 3

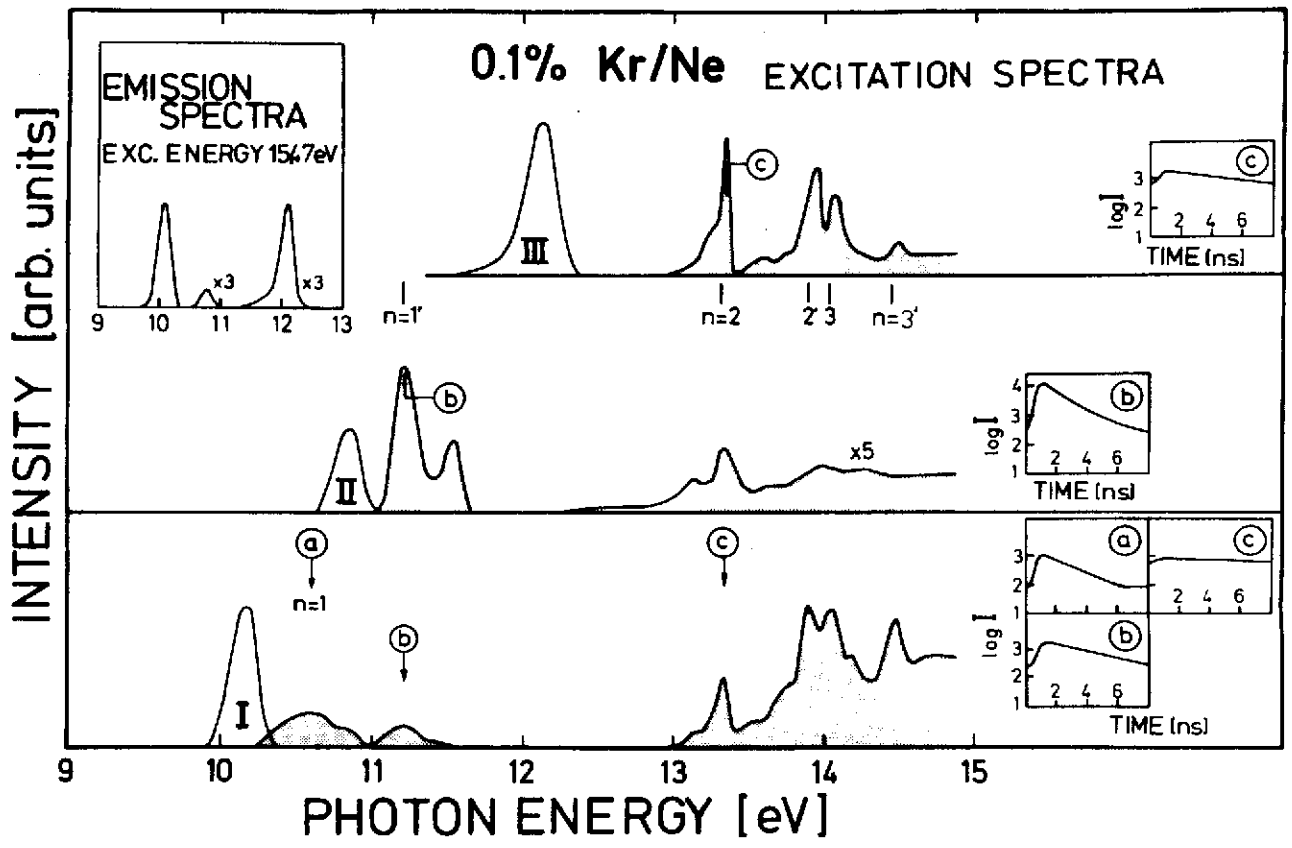
0.1% Kr/Ne EXCITATION SPECTRA
EMISSION SPECTRA
EXC. ENERGY 15.47eV
INTENSITY [arb. units]
PHOTON ENERGY [eV]
TIME (ns)
n=1'
n=2
n=3'
n=1

Fig. 4

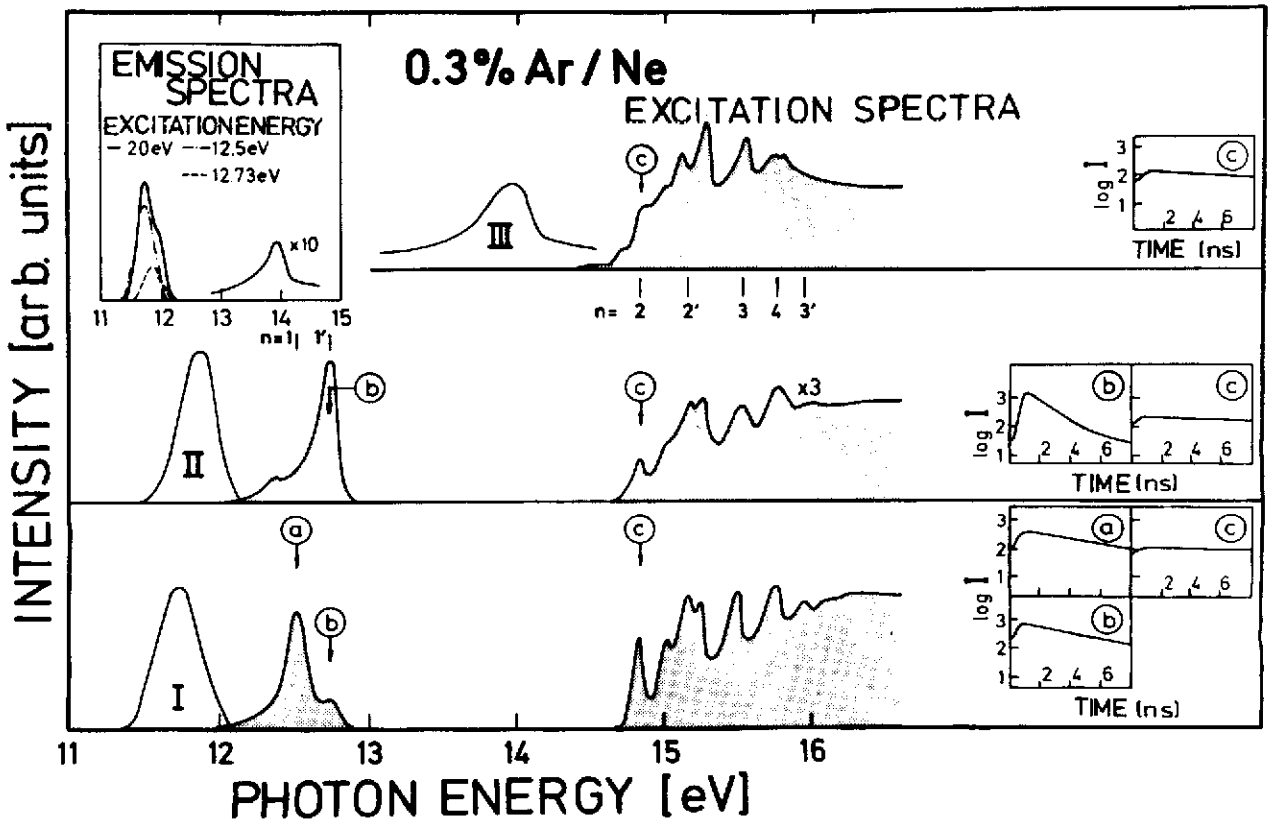
0.3% Ar / Ne
EXCITATION SPECTRA
EMISSION SPECTRA
EXCITATION ENERGY
— 20eV — 12.5eV
--- 12.73eV
INTENSITY [arb. units]
PHOTON ENERGY [eV]
TIME (ns)

Fig. 5

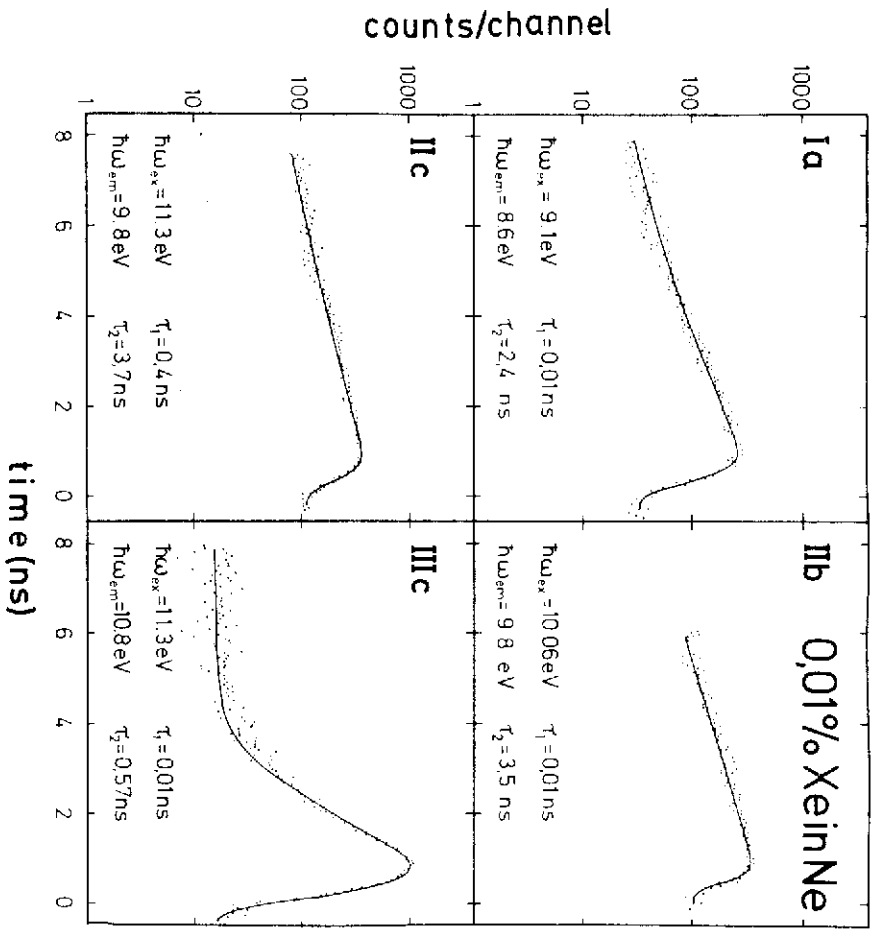
counts/channel
time (ns)
Ia
IIb
0,01% Xe in Ne
IIc
IIIc
ħω_ex = 9.1eV τ1 = 0,01ns
ħω_em = 8.6eV τ2 = 2,4 ns
ħω_ex = 10.06eV τ1 = 0,01ns
ħω_em = 9.8 eV τ2 = 3,5 ns
ħω_ex = 11.3eV τ1 = 0,4 ns
ħω_em = 9.8eV τ2 = 3,7ns
ħω_ex = 11.3eV τ1 = 0,01ns
ħω_em = 10.8eV τ2 = 0,57ns

Fig. 6

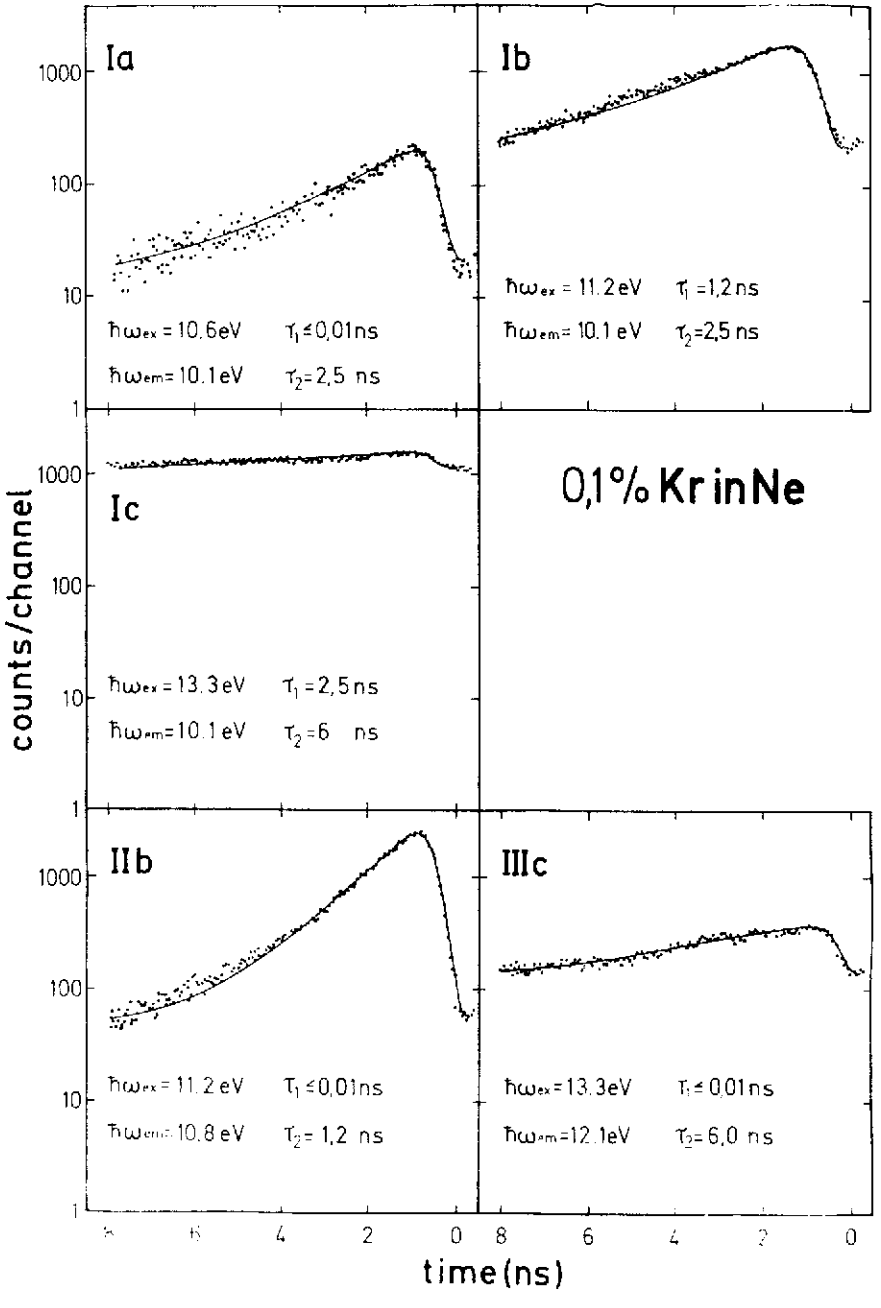
Ia
Ib
Ic
IIb
IIIc
0,1% Kr in Ne
counts/channel
time (ns)
ħω_ex = 10.6eV τ1 ≤ 0,01ns
ħω_em = 10.1eV τ2 = 2,5 ns
ħω_ex = 11.2eV τ1 = 1,2 ns
ħω_em = 10.1 eV τ2 = 2,5 ns
ħω_ex = 13.3eV τ1 = 2,5 ns
ħω_em = 10.1 eV τ2 = 6 ns
ħω_ex = 11.2 eV τ1 ≤ 0,01ns
ħω_em = 10.8 eV τ2 = 1,2 ns
ħω_ex = 13.3eV τ1 ≤ 0,01ns
ħω_em = 12.1eV τ2 = 6,0 ns

Fig. 7

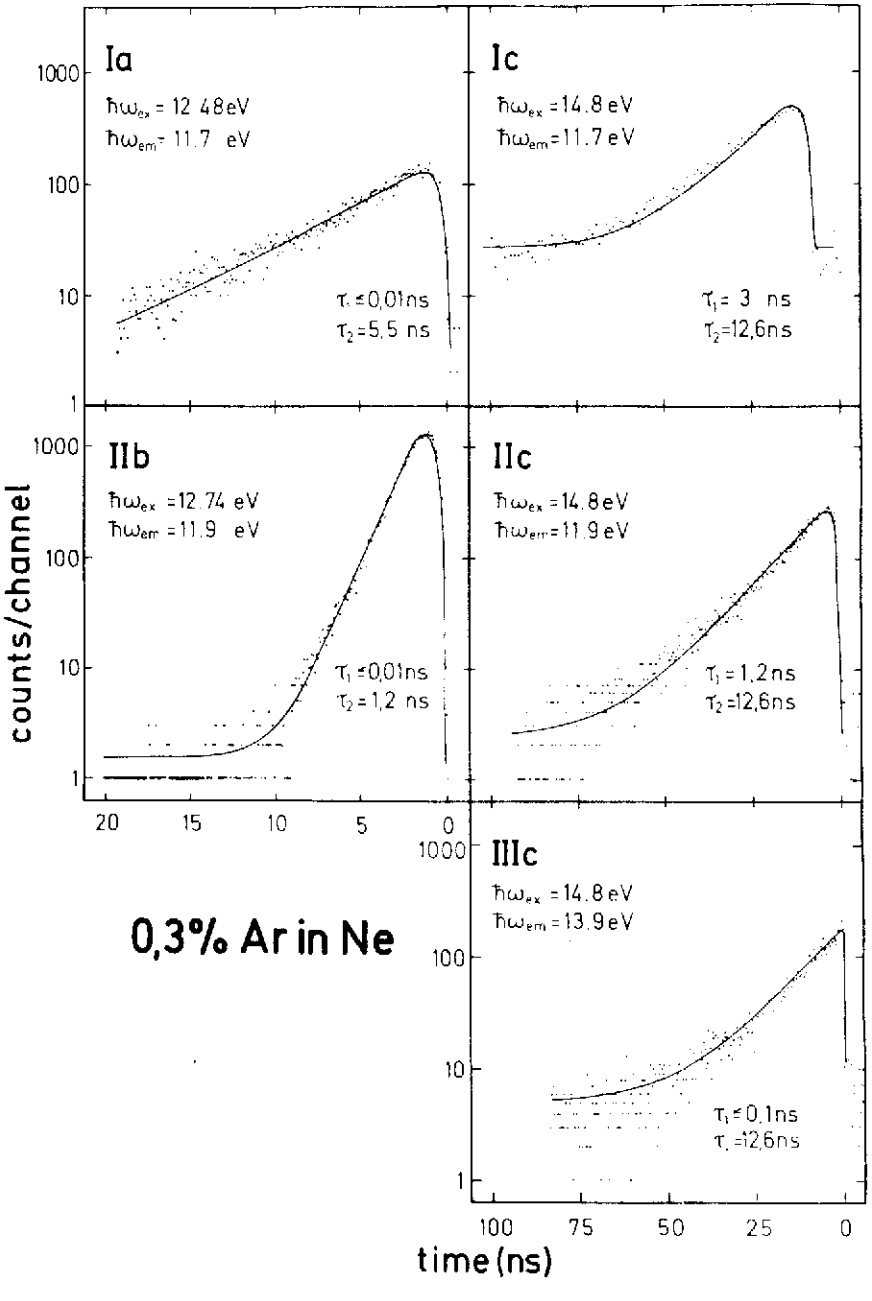
Ia
ħω_ex = 12.48eV
ħω_em = 11.7 eV
τ1 ≤0,01ns
τ2 =5,5 ns
Ic
ħω_ex =14.8 eV
ħω_em =11.7 eV
τ1 = 3 ns
τ2 =12,6ns
IIb
ħω_ex =12.74 eV
ħω_em =11.9 eV
τ1 ≤0,01ns
τ2 =1,2 ns
IIc
ħω_ex =14.8 eV
ħω_em =11.9 eV
τ1 =1,2ns
τ2 =12,6ns
IIIc
ħω_ex =14.8 eV
ħω_em =13.9 eV
τ1 ≤0,1ns
τ2 =12,6ns
0,3% Ar in Ne
counts/channel
time (ns)

Fig. 8

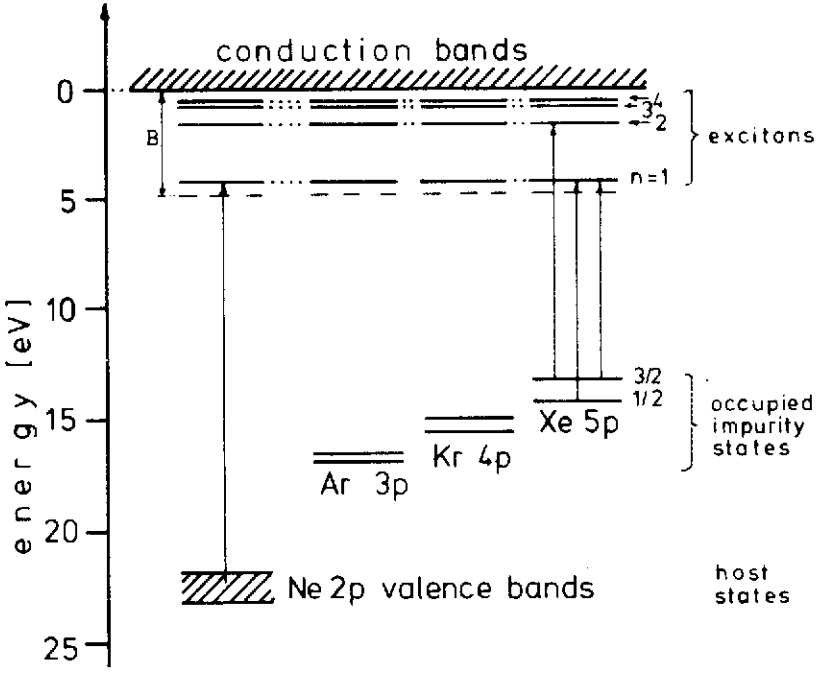
conduction bands
B
3/2
1/2
n=1
excitons
3/2
1/2
occupied impurity states
Xe 5p
Kr 4p
Ar 3p
Ne 2p valence bands
host states
energy [eV]

Fig. 9

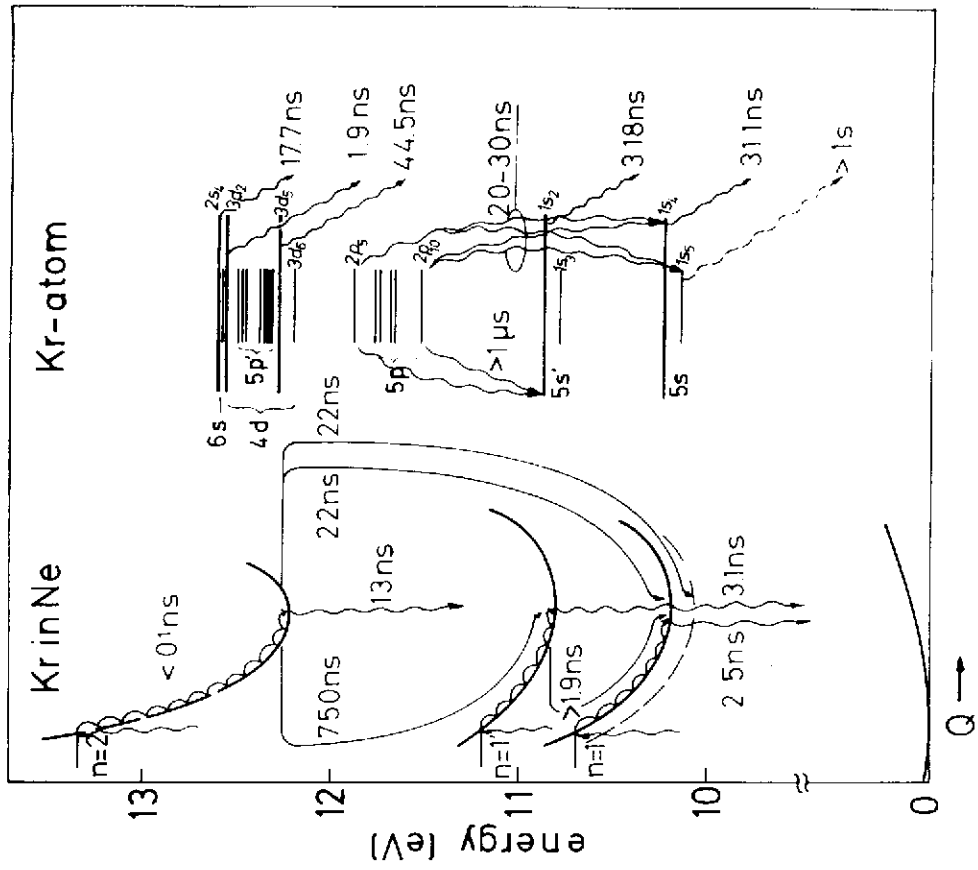
Kr-atom
Kr in Ne
energy (eV)
Q
13
12
11
10
0
6s
4d
5p'
5p
5s'
5s
17.7ns
1.9ns
44.5ns
20-30ns
318ns
311ns
>1s
>1µs
22ns
22ns
13ns
750ns
< 0.1ns
>1.9ns
2.5ns
3.1ns
n=2
n=1
n=1

Fig. 11

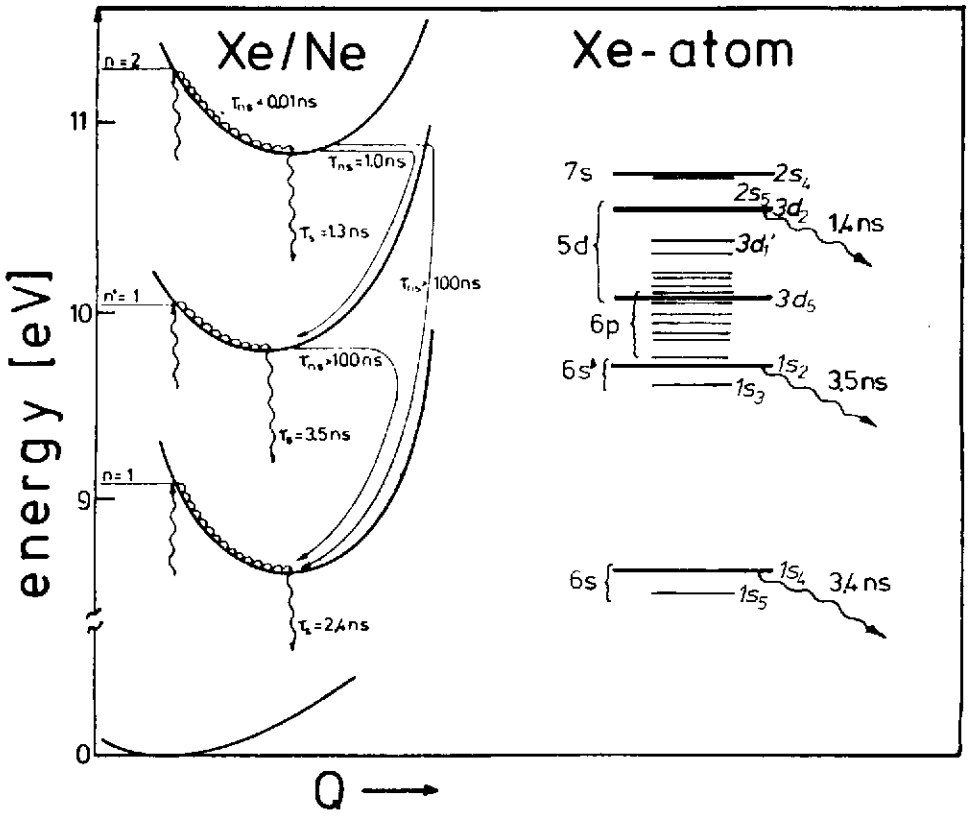
Xe/Ne
Xe-atom
energy [eV]
Q
11
10
9
0
n=2
n*=1
n=1
τ<0.01ns
τ=1.0ns
τ=1.3ns
τ>100ns
τ>100ns
τ=3.5ns
τ=2.4ns
7s
2s4
2s5
3d2
1.4ns
5d
3d1'
3d5
6p
6s'
1s2
1s3
3.5ns
6s
1s4
1s5
3.4ns

Fig. 10

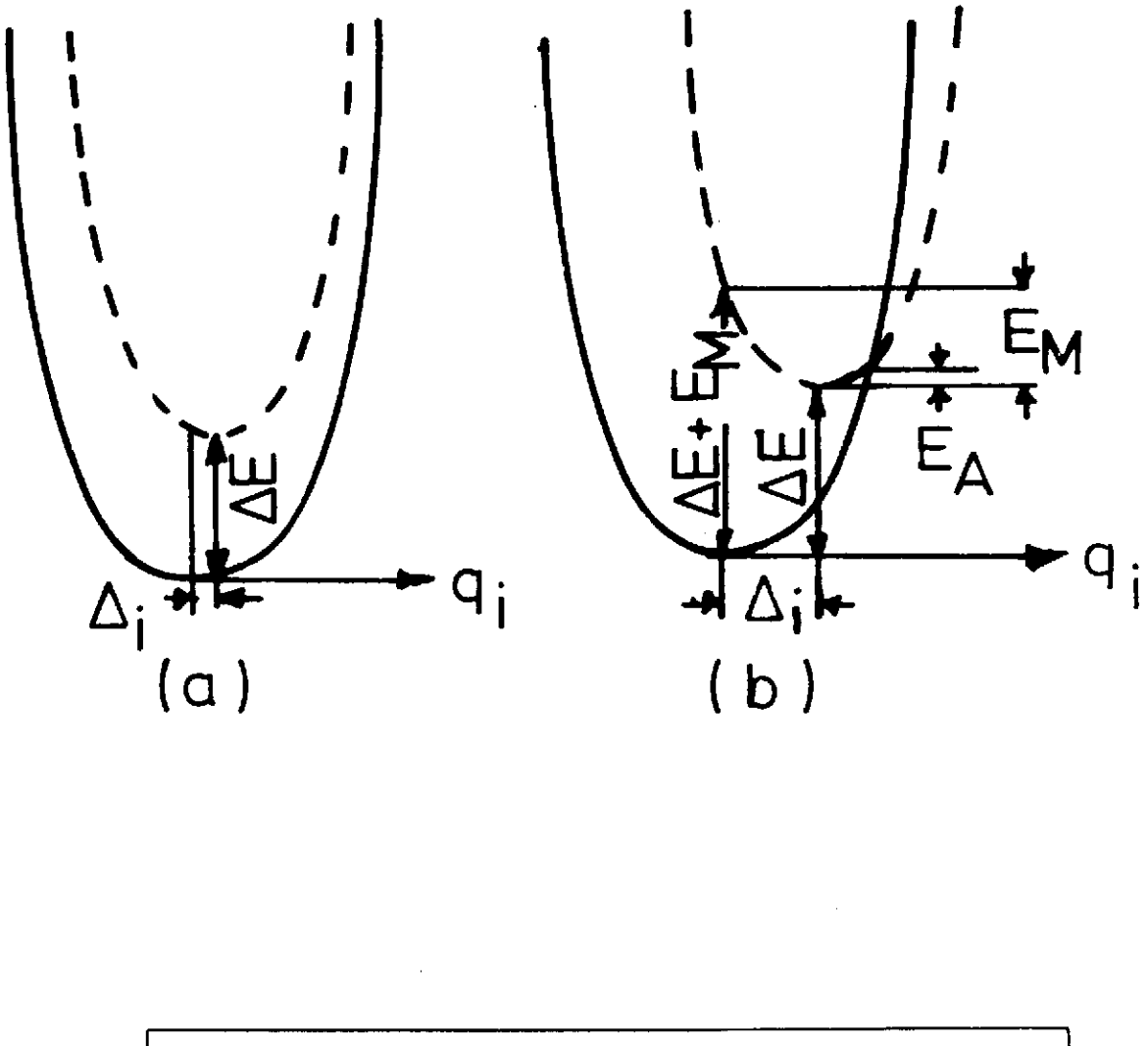
ΔE
Δi
qi
(a)
EM
EM
ΔE
ΔE
EA
Δi
qi
(b)

Fig. 13

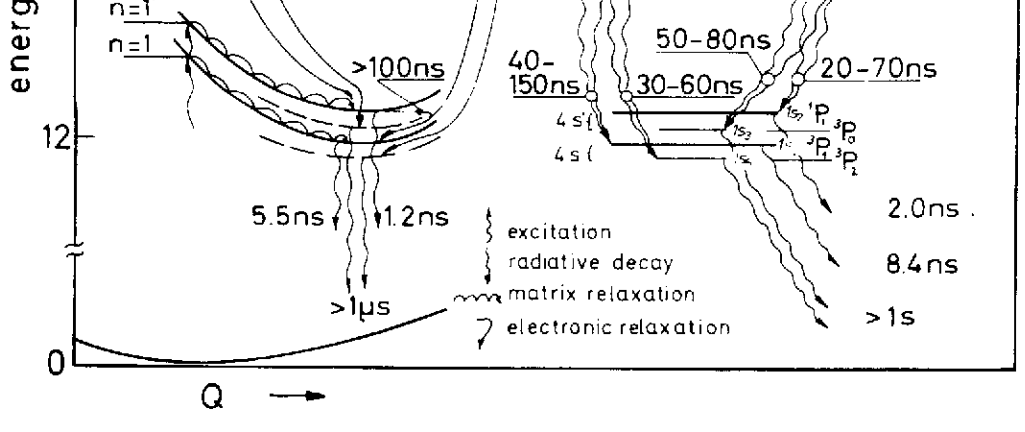
Ar in Ne
Ar-atom
energy (eV)
15
14
13
12
0
Q
n=2
<.01ns
71ns
82ns
63ns
32ns
420ns
n=1'
n=1
>100ns
5.5ns
1.2ns
>1μs
3d
5s
3.7ns
120ns
?
4p'
4p
50-80ns
40-
150ns
30-60ns
20-70ns
4s'
4s
2.0ns
8.4ns
>1s
excitation
radiative decay
matrix relaxation
electronic relaxation

Fig. 12

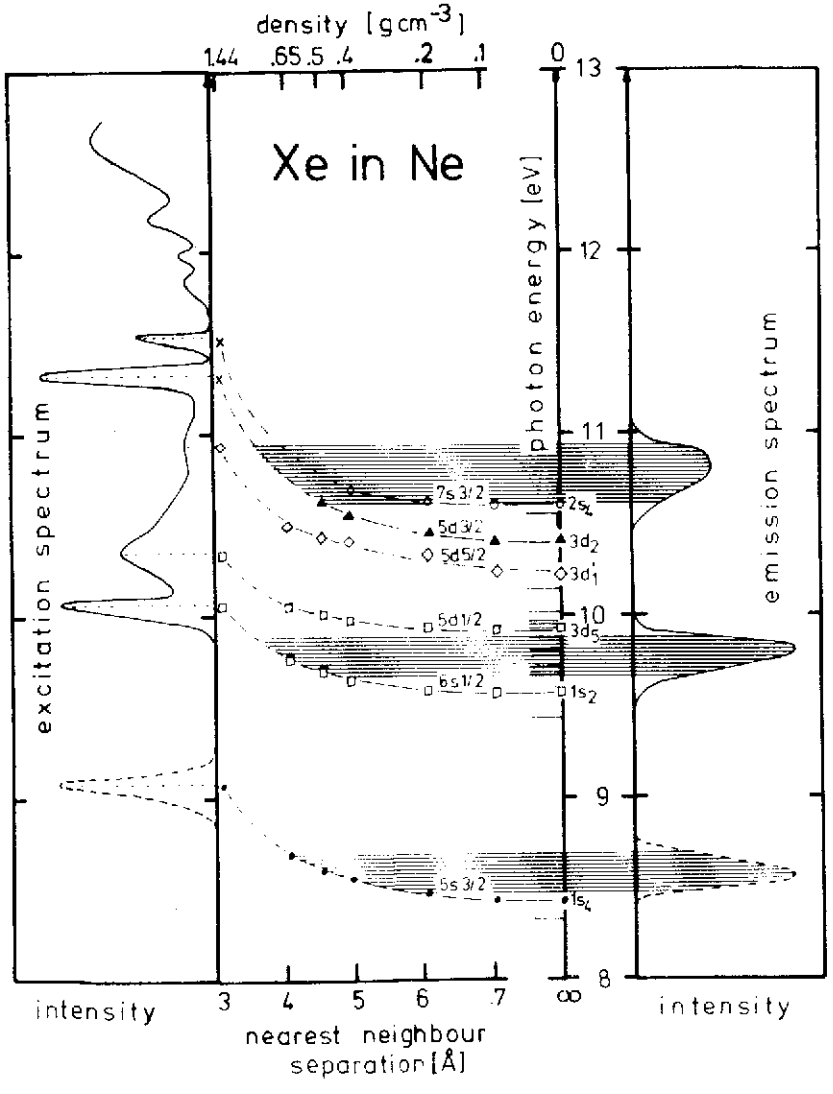
density [g cm^{-3}]
1.44 .65 .5 .4 .2 .1 0
Xe in Ne
photon energy [eV]
13
12
11
10
9
8
excitation spectrum
emission spectrum
7s 3/2
5d 3/2
5d 5/2
5d 1/2
6s 1/2
5s 3/2
2s$_4$
3d$_2$
3d$_1$
3d$_5$
1s$_2$
1s$_4$
intensity
3 4 5 6 7 ∞
nearest neighbour separation [Å]
intensity

Fig. 14

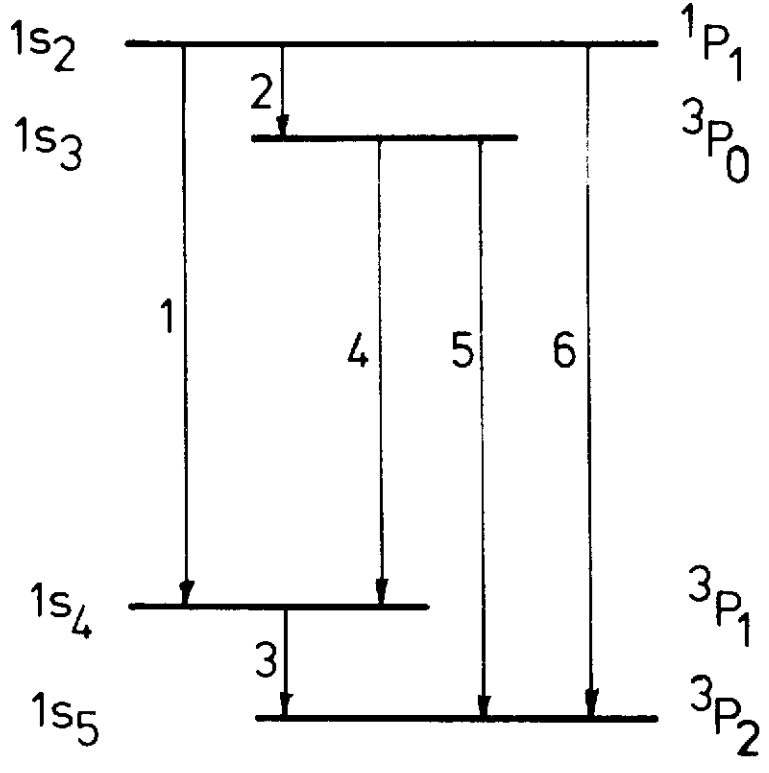
1s$_2$
1s$_3$
1s$_4$
1s$_5$
^{1}P$_1$
^{3}P$_0$
^{3}P$_1$
^{3}P$_2$
1
2
3
4
5
6

Fig. 15

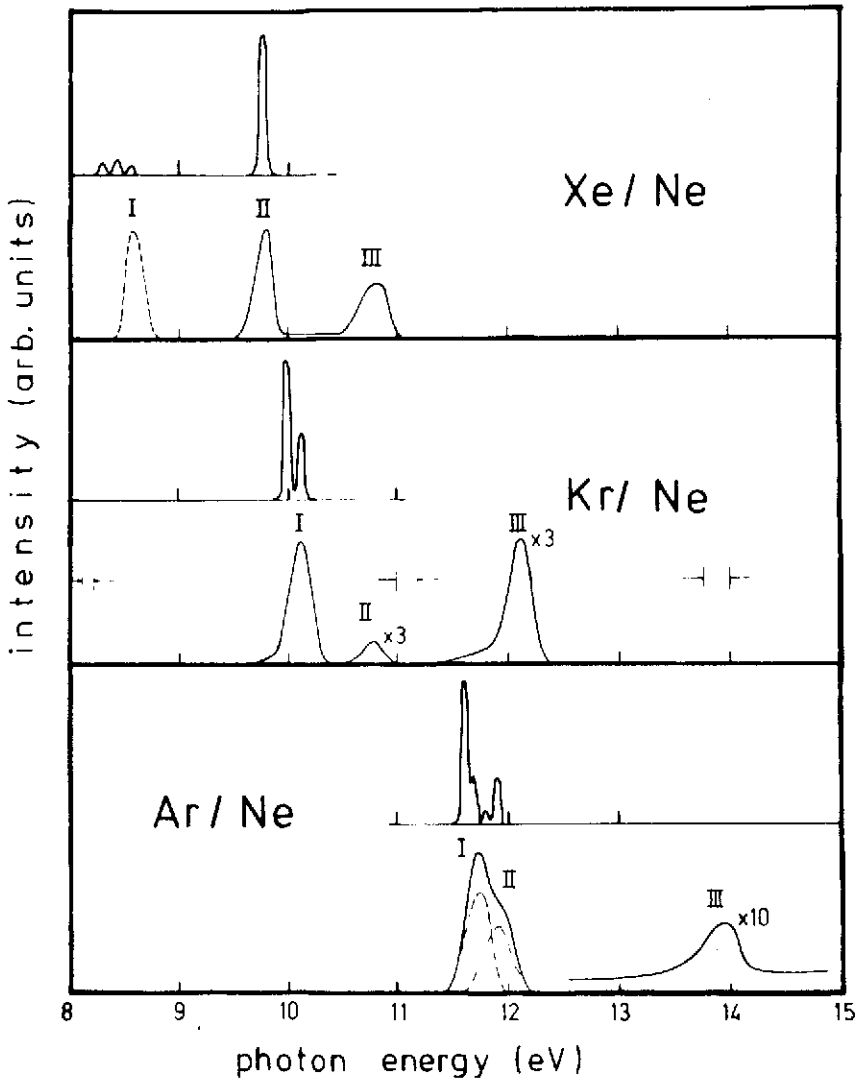
intensity (arb. units)
Xe / Ne
Kr / Ne
Ar / Ne
I
II
III
x3
x10
8
9
10
11
12
13
14
15
photon energy (eV)

Fig. 16

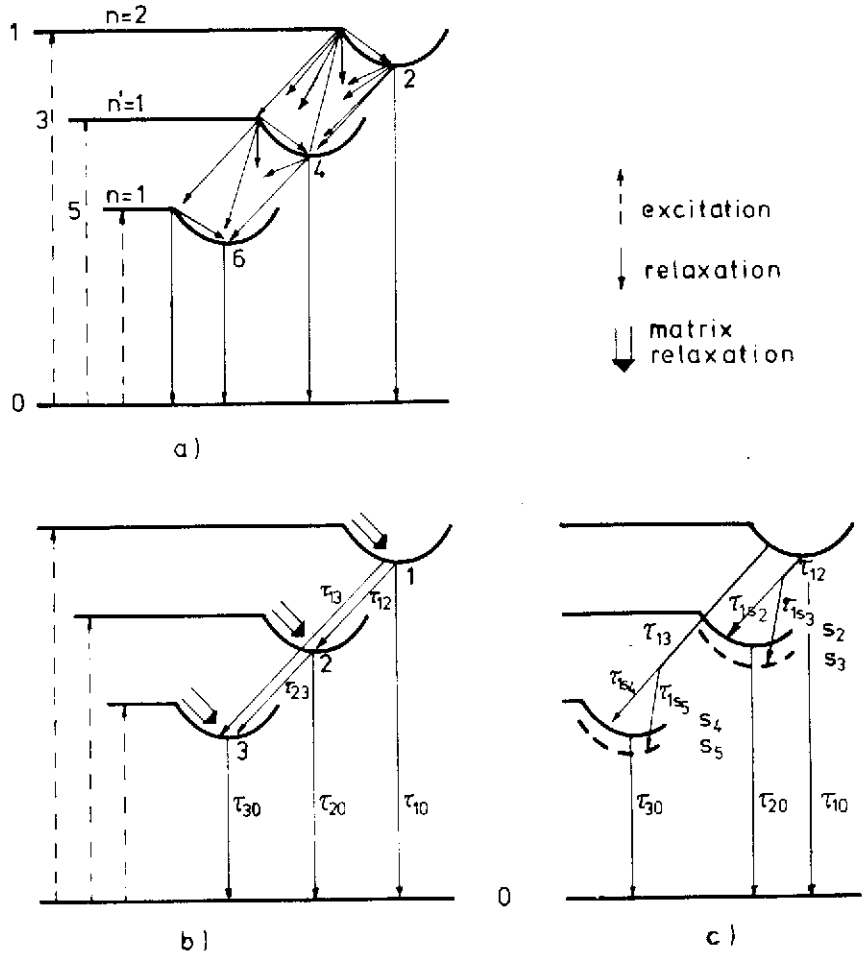
n=2
n'=1
n=1
1
2
3
4
5
6
0
a)
excitation
relaxation
matrix relaxation
τ_{13}
τ_{12}
τ_{23}
τ_{30}
τ_{20}
τ_{10}
b)
τ_{1s_2}
τ_{1s_3}
τ_{1s_4}
τ_{1s_5}
s_2
s_3
s_4
s_5
c)

Fig. 17